THESIS FOR THE DEGREE OF DOCTOR OF PHILOSOPHY

NO_x Formation in Iron Ore Rotary Kilns

Rikard Edland

Department of Space, Earth and Environment
CHALMERS UNIVERSITY OF TECHNOLOGY
Gothenburg, Sweden 2019

NO_x Formation in Iron Ore Rotary Kilns

RIKARD EDLAND
ISBN 978-91-7905-139-6

Doktorsavhandlingar vid Chalmers tekniska högskola
Ny serie nr 4606
ISSN 0346-718X

Department of Space, Earth and Environment
Chalmers University of Technology
SE-412 96 Gothenburg
Sweden
Telephone + 46 (0)31-772 1000

Printed by Chalmers Reproservice
Chalmers University of Technology
Gothenburg, Sweden 2019

NO_x Formation in Iron Ore Rotary Kilns

RIKARD EDLAND
Division of Energy Technology
Department of Space, Earth and Environment
Chalmers University of Technology

ABSTRACT

Iron ore pellets are often produced using the so-called Grate-Kiln process, which is designed to oxidize the magnetite (Fe_3O_4) to hematite (Fe_2O_3) and to sinter the pellets so they can be used in steel manufacturing. The heat required for this process comes from the combustion of a pulverized fuel in a rotary kiln, involving the formation of a jet flame. To oxidize the pellets, large amounts of air are introduced into the kiln, and an air-to-fuel equivalence ratio of 4–6 is obtained. Furthermore, the air is pre-heated to >1000°C. High temperatures and large amounts of excess air are known to promote NO_x formation and NO_x emissions from iron ore processing plants are in general high.

This thesis describes the NO_x formation in the rotary kiln and identifies the governing parameters, with the aim of reducing the emissions. The work involves experiments in a pilot-scale kiln, as well as modeling work based on the same experiments. Data from a full-scale iron ore pelletization plant are also provided.

From the experiments and the modeling work in this thesis, thermal NO is deemed to be of low importance in iron ore rotary kilns when solid fuels are combusted. Instead, the conditions during char combustion contribute significantly to the overall NO_x formation. These results explain why many of the primary measures used to date have failed to achieve reductions in NO_x emissions. Suggested additional primary measures include: raising the pyrolysis temperature (e.g., through oxygen addition) to deplete the char of nitrogen; or switching to a fuel with a lower nitrogen content (e.g., wood pellets). These are interesting alternatives for the future, and the latter may be tested in the coming years.

Keywords: Nitrogen oxides, combustion chemistry, emissions control, rotary kiln, Grate-Kiln process

List of publications

The thesis is based on the following papers, which are referred to in the text according to their Roman numerals:

Paper I. R. Edland, F. Normann, C. Fredriksson, K. Andersson, *Implications of fuel choice and burner settings for combustion efficiency and NO_x formation in PF-fired iron ore rotary kilns,* Energy and Fuels, 2017, 31 (3), pp 3253–3261.

Paper II. R. Edland, F. Normann, K. Andersson, *Modelling the contribution from volatile and char bound nitrogen to NO_x formation in iron ore rotary kilns,* Energy and Fuels, 2018, 32 (2), pp 2321-2331.

Paper III. R. Edland, F. Normann, T. Allgurén, C. Fredriksson, K. Andersson, *Scaling of Pulverized-Fuel Jet Flames That Apply Large Amounts of Excess Air—Implications for NO_x Formation***,** Energies, 2019, 12(40), Article number 2680

Paper IV. R. Edland, N. Smith, F. Normann, T. Allgurén, C. Fredriksson, T. Fletcher, K. Andersson, *Evaluation of NO_x reduction measures for iron ore rotary kilns*, Submitted.

Paper V. R. Edland, T. Allgurén, F. Normann, A. Fry, E. Eddings, K. Andersson, *The relevance of homogeneous and heterogeneous reactions for NO formation in three PF-flame types*, Submitted.

Rikard Edland is the principal author of all five papers. Associate Professor Fredrik Normann and Professor Klas Andersson contributed with discussions and editing for all the papers. Dr. Christian Fredriksson organized the experimental campaign in **Paper I** and provided the industrial perspective in **Papers I**–**IV**. Dr. Thomas Allgurén contributed with discussions and editing of **Papers III–V** and performed the experiments presented in **Paper V**. Professor Tom Fletcher conducted the flat-flame experiments described in **Paper IV**. Neil Smith contributed with discussion and input to **Paper IV**. Professors Andrew Fry and Eric Eddings organized the measurement campaign in **Paper V**.

Additional work has been carried out during the period of the thesis work, as listed below. These papers are not included in the thesis due to either overlap with the appended papers or their being outside the scope of the current thesis.

a) R. Edland, F. Normann, C. Fredriksson, K. Andersson, *Formation of nitrogen oxides in rotary kiln burners: an assessment of pilot scale experiments using gaseous, liquid and solid fuels*, INFUB Conference 2015.

b) R. Edland, F. Normann, K. Andersson, *Nitrogen chemistry in rotary kiln flames: Impact of mixing rate and temperature at high air to fuel ratios*, Nordic Flame Days Conference 2016.

c) R. Edland, T. Allgurén, F. Normann, K. Andersson, *The connection between NOx and soot in oxygen-enriched propane flames*, Clearwater Clean Energy Conference 2018.

d) R. Edland, T. Allgurén, F. Normann, K. Andersson, *Formation of soot in oxygen-enriched propane flames*, Submitted for publication 2019.

Acknowledgments

First of all, I want to express my gratitude to my supervisors professor Klas Andersson and associate professor Fredrik Normann who made this thesis possible. Thank you for entrusting me with this work, for sharing your expertise and for providing me with your valuable guidance. LKAB and the Swedish Energy Agency are acknowledged for their financial support. A special thanks to doctor Christian Fredriksson for productive discussions and a willingness to work together and share data.

I'm very grateful for having Adrian Gunnarsson as a close colleague and now as a close friend. Thank you for the many hours shared in the office and out in the field. A big thanks to Thomas Allgurén for being one of the few people that I can discuss combustion chemistry and video games with, and for acting as a mentor. I am also grateful to the rest of the Combustion and Carbon Capture Technologies group (Dan, Max, Jakob, Rubén, Johanna) for entertaining meetings and interesting discussions. I'm very happy that Angelica Gyllén has been my officemate, thank you for all the interesting discussions we've had and for your moral support. To the rest of Energy Technology: thank you for contributing to a stimulating and fun working environment, and thanks to everyone who organizes board game nights, lunch-running and other events. An extra appreciation goes to the A-team for all the work that you do behind the scenes that enables us to work and have a good time.

Furthermore, thanks to all my friends outside of Energy Technology and Chalmers for making my life so enjoyable, whether it is by playing sports, video games, music or just spending quality time together. You're too many to mention but know that you are loved and appreciated. My family receives my deepest gratitude: my brother for being a great friend and someone that I've looked up to my entire life; my father for always believing in me and my technical skills; and to my mother for the unyielding support and love you always give me.

My final acknowledgement goes to my girlfriend Sofie. Thank you for being by my side and for being the lovely person you are. You light up my life.

Rikard Edland
Gothenburg, Sweden
July 2019

Table of contents

1 Introduction

Air pollution is a topic of major concern that receives considerable attention due to the negative impacts that it has on humans and the environment. It is even a major part of the UN sustainability Goal 7 – *Affordable and Clean Energy*. A solid body of literature [1-7] supports the notion that exposure to air pollution is harmful to the cardiovascular, circulatory and respiratory systems of humans, and thus shortens life expectancy. It is also well-known that vegetation and wildlife suffer because of air pollution [8-10]. Today, the emission of pollutants from conventional combustion processes, e.g., in the automotive industry and the heat and power industry, is strictly regulated in many parts of the world. Emissions from industrial processes that apply less-conventional combustion systems have received less attention and now typically lie above e.g., conventional power plants that apply state-of-the-art technologies. However, this situation is changing, and smaller industrial processes are starting to attract more attention regarding their emissions.

The Grate-Kiln process, applied in the iron ore industry, is an example of an industrial process that is attracting increased attention regarding emissions reductions. The Grate-Kiln process applies combustion of a fuel together with large volumes of pre-heated (>1000°C) air in a rotary kiln, so as to provide heat for the iron ore. These conditions promote the formation of high levels of nitrogen oxide (NO_x). The rotation of the kiln, the combustion conditions, and the requirement for a high-quality product (iron ore pellets) make the implementation of many conventional NO_x mitigation techniques unfeasible. Therefore, it is important to understand and describe accurately the mechanisms governing NO_x formation, so as to identify and evaluate the mitigation possibilities. This has taken on greater importance in recent times as demands for CO_2 level reductions and fuel flexibility have grown, and these drivers may give rise to additional changes in the process. Furthermore, it is important to ensure that any measures applied in pilot-scale are correctly scaled up to the commercial scale.

1.1 Aim

This work characterizes the formation of NO_x in industrial jet flames, specifically in the Grate-Kiln process, with the aim of supporting the development of suitable emission control. A combination of experimental and modeling work is used to investigate the formation of NO_x, as well as to evaluate potential mitigation measures. The importance of scaling is also discussed, as it is an important element in ensuring impact in the full-scale setup. Two key research areas are identified:

A. Characterization of the NO_x formation mechanism in jet flames applied to iron ore rotary kilns.

B. Identification of measures for reducing NO_x emissions in iron ore rotary kilns.

1.2 Outline of the thesis

This thesis consists of a summary and the five appended papers. Chapter 2 places the work in context by presenting the trends in atmospheric pollution and describing the issues with respect to NO_x formation in the iron ore industry. Chapter 3 presents the theoretical framework of the processes that govern NO_x formation. Chapter 4 summarizes the previously conducted research on NO_x mitigation in rotary kilns. Chapters 5 and 6 describe the experimental and numerical methods used. Chapter 7 describes the results and a discussion thereof. The thesis concludes with a summary and some ideas for future work.

The papers upon which the thesis is built are described briefly below.

Paper I is an experimental investigation of the impacts of the fuel characteristics and combustion parameters on NO_x formation in rotary kilns. Four coals, as well as co-firing of coal and biomass were tested in a pilot-scale kiln (580 kW), and several burner settings were investigated.

Paper II assesses the importance of the NO_x formation mechanisms in iron ore rotary kiln flames using detailed reaction modeling, based on the results obtained in **Paper I**. A couple of theoretical NO_x mitigation measures are evaluated.

Paper III is an investigation of how the transition from pilot-scale to full-scale affects NO_x formation in iron ore rotary kilns. Emissions from a full-scale iron ore rotary kiln (40 MW) are compared with those from a pilot-scale kiln (580 kW) for three coals and one heavy fuel oil, and the mechanisms of NO_x formation are discussed with the support from detailed reaction modeling.

Paper IV evaluates NO_x mitigation measures that have been tested over the years in both the pilot-scale kiln and full-scale kiln owned by LKAB, in light of the more recent findings presented in **Paper III**.

Paper V combines experimental and modeling work to evaluate NO_x formation in two staged 1-MW flames and one unstaged 30-kW flame. The effect of flame type on NO_x formation is investigated, and the specific modeling approach that is best suited to each individual flame type is explored.

2 Background

This section places the work of the thesis in context. A brief overview of atmospheric pollution is presented, along with the trends in emissions since Year 1970. Atmospheric pollution is here defined as contamination of the atmosphere and refers primarily to emissions that are directly harmful to humans or the environment, although CO_2 is also included. This is followed by a brief description of the iron ore industry and the Grate-Kiln process.

2.1 Atmospheric pollution

Atmospheric pollution from anthropogenic activities is a worldwide concern. Occasionally, nature produces what is considered a pollutant species of her own, e.g., through lightning or volcanic eruptions. However, human industrial activities generate significantly more pollution over time and tend to concentrate the pollution to areas where humans live [11]. Air pollution from wood-burning fires was an issue already in ancient Rome, and fuel combustion related to the manufacturing of lime, glass and brick resulted in significant pollution during the Middle Ages [12]. The introduction of the steam engine in the 18th Century resulted in a surge of coal combustion and, consequently, a substantial increase in production capacity and pollution. While major advances have been made regarding the mitigation of pollution, industrialization and the development of the internal combustion engine have led to a tremendous increase in fuel combustion worldwide, which means that air pollution poses a major problem in many parts of the world. The World Health Organization states that "*Air pollution represents the biggest environmental risk to health. In 2012, one out of every nine deaths was the result of air pollution-related conditions*" [2].

One of the more direct and well-known consequences of pollution is smog. The visible pollution from combustion, consisting of numerous substances, was mostly referred to as 'smoke' until the 20th Century. The term 'smog', a combination of the words 'smoke' and 'fog', was introduced in 1905 in Great Britain. The 'smoke' part of the word referred to direct emissions from the combustion of coal and raw materials, while the 'fog' part referred to meteorological inversion, whereby the gases closest to the earth surface are trapped (which facilitates fog formation). London was particularly plagued by smog, especially in December 1952 when the 'Great Smog of London' occurred, killing thousands of people, perhaps as many as 12,000 if one counts the high mortality rate in the subsequent months [13]. This type of smog is sometimes referred to as 'London-type smog' and is a direct consequence of the incomplete combustion or usage of dirty fuels. Such emissions, i.e., emissions that are emitted directly from the combustion process, are designated as 'primary emissions'. Since the 1950s, London-type smog has been reduced in most cities in the Western world, partly due to the achievement of higher combustion efficiencies and the reduced use of coal for domestic heating, but also due to industries designing taller smokestacks (i.e., emitting at higher altitude) [14]. Today, another type of smog, 'photochemical smog', is commonly seen in many cities, with Los Angeles being a prime example. Several of the constituents of photochemical smog are formed through chemical reactions that occur between primary emissions and the atmosphere and that are activated by sunlight (hence 'photochemical'). Such pollution is often referred to as 'secondary emissions', since the main pollutants are not formed during the combustion process itself. The key ingredients of photochemical smog are nitrogen oxide, hydrocarbons, and sunlight, while the most hazardous components of photochemical smog are ozone and particulate matter [15].

Another major air pollution problem is acid deposition, in the form of either acid rain (wet deposition) or gas and particles (dry deposition). Oxides of sulfur (SO_x) and oxides of nitrogen (NO_x) that are released into the atmosphere can form acidic compounds, which can be transported thousands of kilometers before being deposited. The resulting acidification of soil

and waterways is harmful to the vegetation and aquatic wildlife, and has caused severe environmental problems in many parts of the world [10]. Scandinavia and parts of Germany were particularly affected by acid rain during the period 1955–1970, and even though acid rain is not as problematic today (Year 2019), many lakes are still being treated with lime in order to adjust the pH-value of the water so that it can sustain life [16, 17].

The global emissions of NO_x, SO_x, $PM_{2.5}$ and CO_2 in the period of 1970–2012 (2017 for CO_2) are presented in Figure 1, based on the information in the EDGAR database [18, 19]. The global NO_x emissions have increased steadily, although Europe and the US have managed to reduce their emissions. Global SO_x emissions decreased between 1980 and 2000, although since Year 2000 they have been rising again, mainly due to increased coal combustion in China and India, as well as an increase in global shipping. For the global $PM_{2.5}$ emissions, i.e., particulate matter with a diameter of <2.5 µm, a similar trend has been observed. It should be mentioned that the $PM_{2.5}$ data are based on the usage of fossil fuels. If biofuels are included, the emissions become significantly higher due to domestic heating in many regions, especially in India and the "Rest of the world". CO_2 emissions, which are also based on the combustion of fossil fuels, have seen the most dramatic increases over the selected time period. In general, there is a distinct correlation between CO_2 emissions and emissions of pollutants such as NO_x, SO_x and PM. The main reason for the relatively larger increase in CO_2 emissions is that the other pollutants can currently be controlled through combustion modifications (so-called 'primary measures') or flue-gas cleaning ('secondary measures'), while the capture of CO_2 is not yet implemented on a significant scale.

As mentioned above, Europe and the US have managed to reduce their emissions of NO_x, SO_x and $PM_{2.5}$. However, many Western industries are struggling to comply with new and more stringent regulations. The energy sector and the transport sector have received a lot of attention as they are the largest emitters. This has resulted in the development of primary and secondary measures suited to, for example, boilers and engines. However, other industrial processes have received less attention but often have significantly higher emissions than conventional combustion plants.

The iron ore industry is in need of mitigation technologies that are adapted to its processes, especially with respect to the generation of NO_x. For SO_x and PM, secondary measures are the go-to alternative: they are relatively straightforward to implement albeit costly. For NO_x, primary measures are always preferred due to the cost of secondary measures. This applies even more to iron ore pelletization plants, since the large flow of flue gases and the dusty environment make secondary measures for NO_x difficult to operate. However, primary measures that are tailored to these processes have not yet been developed, so NO_x emissions remain high. According to the Swedish Environmental Protection Agency (*Naturvårdsverket*), the top two point-sources of NO_x emissions in Sweden are iron ore pelletization plants (as of Year 2018) [20]. It should also be mentioned that although there is currently a correlation between CO_2 emissions and other pollutants, it is not necessarily the case that the levels of NO_x will decrease if the CO_2 levels are decreased. Alternatives to fossil fuels, e.g., biomass, hydrogen, or high-temperature electrification using plasma torches, may still generate significant amounts of pollutants (especially NO_x).

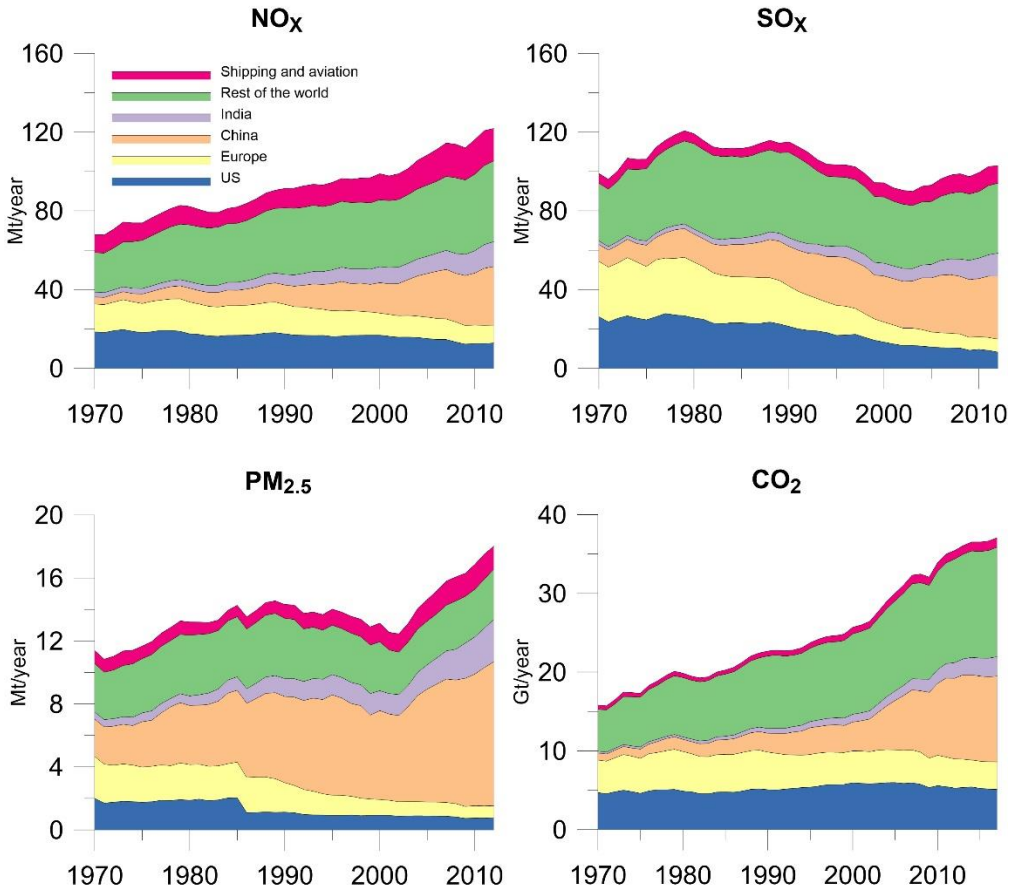

Figure 1. Global emissions of NO_x, SO_x, $PM_{2.5}$, and CO_2 (from fossil use). Note that the *y*-axis for CO_2 is in units of Gt/year. Data are taken from the EDGAR database [18, 19]

2.2 Iron ore industry

The main consumer of iron ore is in primary steelmaking. Since the Year 1950, the annual steel production level has risen from 189 tonnes/year to 1,808 tonnes/year (Year 2018), with 50% of this increase occurring since Year 2000 [21]. Postindustrial countries show a tendency towards saturation of the steel demand when the in-use stock of steel is around 13 tonnes/capita [22], i.e., not much new steel has to be produced once this is achieved. Countries that are undergoing industrialization initially have a lower in-use stock of steel (in Year 2005, China and India had stocks of 2.2 and 0.4 tonnes/capita, respectively[23]). However, they are likely to eventually increase their steel stocks to around 13 tonnes/capita, so a continued global demand for primary steel is expected. Thus, the demand for iron ore will also remain high.

In the steelmaking industry, two forms of iron ore are used: sinter and pellets. Pellets are often preferred in both the steelmaking process and during transport due to their characteristics (e.g., geometry and strength) [24]. For the production of iron ore pellets, there are two main processes: the Straight-Grate process, and the Grate-Kiln process. The advantages and disadvantages of each process are discussed in the work of Zhu et al [25], with references to Mourão et al [26]. However, both processes emit large amounts of NO_x. The Swedish iron ore industry is dominated by the company Luossavaara-Kiirunavaara Aktiebolag (LKAB). The amount of NO_x from LKABs Grate-Kiln plants are in the range of 150–175 g/tonne pellets, according to available literature from Year 2006 [27]. Straight-Grate plants produce slightly higher levels of NO_x. The emissions from the Swedish plants are, however, lower than those from pelletization plants in many other regions [28], although still high if compared with, for

example, power generation on a g/MJ_{fuel} basis. This thesis focuses on the Grate-Kiln process, which is described in the following section.

The Grate-Kiln process

A schematic of the Grate-Kiln process is shown in Figure 2. While different manufacturing plants may have slightly different configurations, the overall layout is the same. The green (unprocessed) pellets are fed onto the grate, where they are dried and preheated by the recirculated hot air flows from the cooler. The grate is divided into zones that receive air from a corresponding zone in the cooler. If the iron ore contains magnetite (Fe_3O_4) a significant amount of heat is released by its oxidation to hematite (Fe_2O_3), which occurs in the later stages of the grate (TPH and PH in Figure 2). By the time they reach the end of the grate, the pellets are of sufficient strength to be introduced into the rotary kiln, where they are sintered. The kiln is slightly tilted, so that the pellets gradually move forward under gravity. Owing to the rotation of the kiln, the pellets are thoroughly mixed, so that a uniform final product is obtained. The heat required for sintering is transferred to the pellets by a flame, usually involving the combustion of coal, although oil and gas are also used. The hot sintered pellets then proceed to the cooler where they are cooled by ambient air. The warm air that exits the cooler is used for preheating the pellets on the grate and as combustion air in the kiln. The air used in the kiln comes from the first part of the cooler (C1 in Figure 2) and may have a temperature of >1100°C at the inlet, which is significantly higher than the preheating temperature range of 300°–400°C that is typical for the combustion air in heat and power generation plants. Although most of the oxidation of the pellets occurs on the grate, it is important to maintain high levels of oxygen in the kiln, to ensure a high degree of oxidation and to prevent reduction back to magnetite. Thus, a large volumetric flow of air from C1 is needed. Relating the air flow to the fuel flow, an air-to-fuel equivalence ratio of 4–6 is obtained in the kiln, which is significantly higher than the equivalence ratio (of approximately 1) seen in conventional solid fuel combustion.

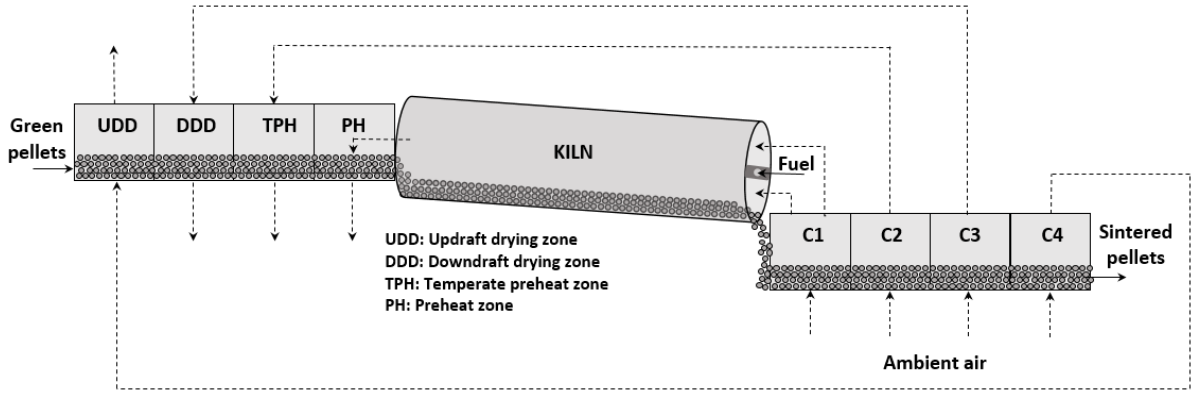

Figure 2. Schematic of the Grate-Kiln process. The dotted lines indicate the gas flows through the process. C1–C4: Cooling sections.

3 Theory

Combustion is a complex process that involves numerous chemical reactions. For simplicity, the written formulas are often representative of the overall reactions and only include the initial reactants and final products. An example of this is the complete oxidation of methane:

$$CH_4 + 2O_2 \rightarrow CO_2 + 2H_2O \qquad \text{R 3-1}$$

In reality, a myriad of intermediate reactions occurs, involving hundreds of intermediate species (e.g., CH_3, OH, HO_2, CO). Some of these species are relatively stable (e.g., CO), while others are unstable (e.g., OH) and react rapidly with other compounds. The unstable species are mainly radicals, i.e., they have an unpaired valence electron. Radicals are crucial to understanding the progress of combustion, and they also govern the formation of pollutants during combustion. The main bulk of the fuel ends up as CO_2 and H_2O, regardless of how the combustion progresses (as long as enough oxygen is available). In contrast, reactive nitrogen species will be converted to NO_x or N_2 depending on the progress of the combustion process and the distribution of radicals. The distribution of radicals reflects the reaction rates of the relevant reactions, which in turn are dependent upon the rate constants and the availability of reactants. The rate constant is most commonly described by the modified Arrhenius expression (although other expressions exist for e.g. surface reactions):

$$k = AT^n e^{-\frac{E_a}{RT}} \qquad \text{Eq. 1}$$

where k is the rate constant, A and n are constants that describe the pre-exponential factor, T is the temperature, E_a is the activation energy, and R is the gas-law constant. For many reactions, n is equal to zero. Mathematically, this expression gives that the rate constant (and thus the reaction rate) increases exponentially with temperature, as long as the activation energy is above zero and the temperature is less than the value of $E_a/2R$. A high activation energy equals low rates at low temperatures.

3.1 NO formation

NO_x is a term that groups nitric oxide (NO) and nitrogen dioxide (NO_2), and sometimes nitrous oxide (N_2O). In this work, only NO and NO_2 are included in NO_x. NO_x is dominated by NO at the high temperatures of combustion processes. Therefore, research on NO_x is concerned with the formation and destruction of NO rather than of NO_2. However, the emitted NO rapidly converts to NO_2 at lower temperatures. This chapter describes the chemistry of NO during combustion and considers the influences of various combustion parameters. The focus here is on solid fuel combustion, as solid fuels are the most commonly used in the Grate-Kiln process.

NO may be formed from either the nitrogen introduced with the air (N_2) or the nitrogen introduced with the fuel (fuel-N). When firing gaseous or liquid fuels, it may be assumed that all or most of the generated NO originates from N_2, due to the absence or low level of fuel-N. In contrast, fuel-N is usually the main contributor to NO in solid fuel combustion [29]. Although NO formation is complex and includes hundreds of intermediate reactions, it is – for pedagogic purposes – common to split the process into three main mechanisms:

- Thermal NO formation – reaction between N_2 and O_2 to form NO
- Prompt NO formation – reaction between N_2 and fuel radicals to form NO
- Fuel NO formation – oxidation of fuel-N to form NO

Thermal NO formation, as the name suggests, is dependent upon a high temperature, since the N_2 molecule contains a strong triple bond that requires large amounts of energy for breakage. The mechanism underlying thermal NO formation was first proposed by Zeldovich (after whom the mechanism is named) [30]. Originally, the Zeldovich mechanism involved the two reactions R 3-2 and R 3-3, while a third reaction, R 3-4, was added later:

$$N_2 + O \leftrightarrow NO + N \quad \text{R 3-2}$$

$$N + O_2 \leftrightarrow NO + O \quad \text{R 3-3}$$

$$N + OH \leftrightarrow NO + H \quad \text{R 3-4}$$

Thermal NO formation is limited by the forward reaction of R 3-2, and once activated, it promotes the other reactions by providing N-radicals. The activation energy of R 3-2 is approximately 318 kJ/mol. Typically, the formation rate of thermal NO becomes significant, relative to other NO reactions, at around 1800 K, although the concentrations of all the included species are important for determining the eventual rate. The gas residence times at these high temperatures are also important in terms of the total amount of NO produced by the thermal mechanism.

Prompt NO formation converts N_2 into NO through an initiating reaction between a CH-radical and an N_2 molecule, to form NCN. The number of relevant reactions for this far exceeds the number of reactions involved in thermal NO formation, which means that prompt NO formation is significantly more complex. While prompt NO formation is rapid (hence its name), it is only active in the presence of short-lived hydrocarbon radicals. It can play an important role in hydrocarbon flames, although it is expected to be negligible when fuel-bound nitrogen is present [31]. As this thesis focuses on solid fuel combustion (with fuel-bound nitrogen), prompt NO will not be explicitly discussed, although considered in the simulations.

Fuel-N conversion is discussed in detail in the next section. In brief, the fuel-bound nitrogen ends up either as NO or N_2, depending on the local conditions during the combustion process. In particular, the air-to-fuel equivalence ratio, λ, is important for fuel-N conversion. While considerable progress has been made in understanding fuel NO formation [32], it includes many different processes and is, to say the least, challenging to describe. Empirical data are still needed to describe the formation, especially regarding the interactions between the solid and gaseous phases.

Although it is convenient to define NO formation in this manner, these are not mutually exclusive mechanisms. An illustrative example is R 3-2, which ably describes thermal NO production as long as there are no other sources of NO. However, when NO is already present (from, for example, the oxidation of fuel-N) the equilibrium of this reaction is shifted to the reactant side in line with Le Chatelier's principle, thereby reversing the reaction. According to the work of Pershing and Wendt [29], temperatures above 2000 K may be required for thermal NO to contribute significantly in PF flames. Given these types of interactions, determining the contribution of each NO mechanism to the total NO formation is not a trivial task.

3.2 Fuel-N evolution during solid fuel combustion

A solid fuel particle undergoes several processing steps during combustion. In a pulverized fuel (PF) flame, the particle is heated through convection and radiation from the upstream flame as well as the walls, and the water contained in the particle starts to evaporate. For small particles, as in PF flames, this process occurs rapidly (in a couple of milliseconds). Once the drying is completed, the particle temperature increases, the particle starts to decompose, and volatile compounds within the particle escape from the solid fuel matrix. This process is called

'devolatilization' or 'pyrolysis', depending on whether oxygen is present or not. For bituminous coal particles, significant pressure builds up inside the particle, which causes the particles to swell or fracture. The products of devolatilization are volatiles and char. The volatiles, which comprise light-weight gases (such as CO and CH_4), and the tars (heavier hydrocarbons) react with oxygen to form a small flame envelope around the remaining particle. The processes of devolatilization and volatile combustion occur on a time-scale similar to that of the drying process. The solid fraction of the particle that remains after devolatilization is the char, which consists mainly of carbon and ash, although small amounts of other elements are also present. When the combustion of volatiles is complete and the flame envelope has disappeared, oxygen reaches the surface of the char and may diffuse into the pores. Heterogeneous reactions between the solid and the gaseous oxygen occur, and the products consist mainly of CO and CO_2. The time-scale for char combustion is considerably longer than those of the previous processes, and usually takes hundreds of milliseconds to reach completion. Other gases, such as H_2O and CO_2, may also react with the solid char. In this case, gasification rather than combustion of the char occurs.

The fuel-bound nitrogen is released either with the volatiles or with the char, and the degree of conversion to NO or N_2 will depend on the local conditions. The following sections cover the partitioning of nitrogen between volatiles (vol-N) and char (char-N) and the formation of NO from vol-N and char-N. Thereafter, the reduction of NO is discussed.

Nitrogen partitioning during pyrolysis

The partitioning of nitrogen during pyrolysis is important for NO formation, since the combustion process and the possibility for NO_x control differ substantially between volatile- and char-bound nitrogen. Even though different conditions yield different volatile products, there is consensus regarding the importance of the pyrolysis temperature in dictating the amount of fuel-N that is retained in the char. Figure 3 presents the percentages of nitrogen that are lost with the volatiles during pyrolysis, based on the studies of Zhang and Fletcher [33], Blair et al [34], Pohl et al [35], Solomon and Colket [36], and Kambara et al [37]. Even though there is a clear trend showing that more nitrogen leaves with the volatiles at higher pyrolysis temperatures, there are considerable differences between the test series. Blair et al [34] have also compared the release rate of nitrogen to the release rate of total mass (which also increases with temperature) during pyrolysis, and have concluded that nitrogen release is more sensitive than mass release to temperature.

As is evident from the variability of the data points in Figure 3, the fraction of nitrogen that leaves as vol-N is not predictable when it is based solely on the pyrolysis temperature. Kambara et al [37] have stated that it is impossible to predict the partitioning of volatile nitrogen based on proximate and ultimate analyses, given their finding that two coals with the same levels of nitrogen and volatile matter yielded two different fractions. However, several models have been subsequently developed that show reasonable success in predicting the composition and yield of volatiles based on the chemical structures of the coals. Three commonly used pyrolysis models are: FG-DVC [38], FLASHCHAIN [39], and CPD [40].

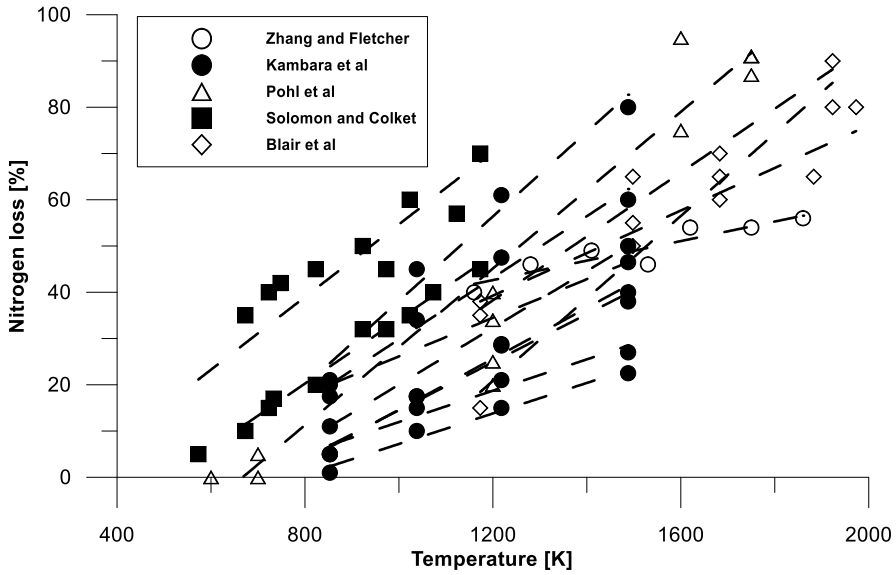

Figure 3**.** Nitrogen loss as a function of pyrolysis temperature. The data are taken from the indicated publications [33-37]. Trend lines are shown for each investigated coal.

Vol-N conversion

The nitrogen-containing volatiles (vol-N) evolve mainly as light-weight nitrogen species (HCN or NH_3), either directly from the coal matrix or indirectly from the tar formed during pyrolysis. Thereafter, they react with radicals to form either NO or N_2. The conversion of light-weight nitrogen gas species to NO is largely dependent upon the availability of oxygen. The conversion can vary from 0% to 100% depending on the local conditions [35, 41]. Thus, if left uncontrolled, vol-N can be a significant contributor to the total NO formation. Given that local stoichiometry has such a strong impact, it is beneficial to design burners and combustion equipment so as to create oxygen-lean combustion zones, thereby reducing the net NO formation. Miller and Bowman [42] have carried out a thorough assessment of the oxidation of light-weight nitrogen species, and the major reaction pathways for HCN and NH_3 have been confirmed: nitrogen atoms in HCN or NH_3 end up as N radicals, which then react either with OH to form NO or with NO to form N_2. In other words, when N radicals are formed, the reactions with NO and with OH compete with each other to form either N_2 or NO. The rate constants of these reactions are usually of similar magnitude, and the yields of NO and N_2 are, thus, a function of the ratio of the OH concentrations to the NO concentration.

Several detailed reaction mechanisms have been proposed for the homogeneous interplay between hydrocarbon combustion and NO formation. The best-known of these is the GRI-Mech mechanism [43], which has been widely used and refined in more recent studies. Such detailed mechanisms are capable of describing the premixed gas flame chemistry with high accuracy. A common approach is to assume that all of the vol-N is released as HCN or NH_3 and, thereafter, converted to NO and N_2, depending on the local gas-phase conditions.

Nitrogen-containing volatiles that are not directly released from the coal matrix or from the tar will be incorporated into the soot that is formed. The reported values for the fractions of volatile nitrogen components trapped in the soot are generally low, even though they may reach up to 30% [44-46]. The importance of soot-bound nitrogen is not well understood. Soot itself can effectively reduce the levels of NO [47, 48], although incorporated soot-N means that there are lower concentrations of light-weight nitrogen gas species that are susceptible to primary NO_x reduction measures.

Char-N conversion

Since it is possible to reduce the conversion of vol-N to NO using controlled mixing of the oxygen and fuel, the oxidation of char-N has grown in importance relative to the formation of NO as the development of low-NO_x burners has evolved. Phong-Anant et al [49], using a drop tube reactor at different temperatures and stoichiometric ratios, found that for fuel-lean PF combustion conditions (λ = 1.25– 1.67, T = 1673–1773 K), vol-N contributed more to the total NO formation than did char-N. In the case of fuel-rich combustion (λ < 1), the contribution of char-N was in the range of 60%–90%. Although char-N conversion has been extensively studied, the results are not as conclusive as for vol-N. One challenge is to differentiate between intrinsic char-N conversion, i.e., the selectivity of char-N towards NO (prior to its reduction by the char), and apparent char-N conversion, i.e., the net conversion after NO reduction by char. As NO is usually measured when the combustion process is completed, data for apparent char-N conversion are more common in the literature than data for intrinsic char-N conversion. Table 1 presents several char-N conversion values obtained under conditions relevant to flame combustion. The values vary within the range of 10%–100%. Different ideas have been put forward to explain this variability. Most of the experimental studies performed [50-54] have noted an increase in char-N conversion with increasing level of stoichiometry, although the magnitude of the observed increase varies between studies. Jensen et al [55] found that the conversion of char-N to NO was close to 100% when very small samples of char (<1 mg, to minimize the NO-char reduction) were combusted at 1323 K and 1423 K, whereas for combustion at 1123 K the conversion of char-N to NO was 65%. The conversion decreased rapidly when the sample size was increased. The availability of O_2 did not affect the conversion for small samples. These results imply that intrinsic char-N conversion is 100% for coal chars at high temperatures, and that NO reduction by char is responsible for the lower values of char-N conversion. A similar study has shown that the parent fuel also plays an important role, as biomass chars showed lower char-N to NO conversion than coal chars [56]. In agreement with Jensen et al [55], Molina and colleagues [53] found a decrease in char-N conversion when the char sample size was increased (≈4.5–21.0 mg). Furthermore, they performed two types of experiments that resulted in two significantly different levels of char-N conversion. In the first (Type I) experiment, the char was first injected into a helium atmosphere and pyrolyzed (low levels of NO and CO exited the char) for 60 s, and then an O_2/He mixture was injected to initiate combustion. In the second (Type II) experiment, the char was injected directly into a stream of O_2/He. The Type I experiment resulted in char-N conversion values in the range of 10%–15%, while the corresponding values in the Type II experiment were in the range of 40%–55%. The authors attributed this difference to a lower local stoichiometry in the Type I experiments leading to an increase in a homogeneous reduction mechanism that involves HCN. Although the importance of HCN for char-N conversion has not been established, modeling conducted by some groups (see for example [57, 58]) have shown that assuming HCN to be the primary product from char-N can provide good results. Another, perhaps more common, approach is to use NO as the primary product obtained from char-N, with subsequent reduction by char.

Additional combustion issues are discussed by Shimizu et al [59], who have shown that the conditions during char production affect the final conversion of char-N to NO. Spinti and Perching [51] have taken this as an explanation for the differences observed in the literature. Jensen et al [55] have shown that NO-char reduction occurs significantly faster directly after pyrolysis than when the char has been prepared separately, as is the case in most NO-char reduction studies.

Table 1. Experimental values for char-N conversion to NO relevant to pulverized coal combustion, as obtained from the literature.

Reference	Apparatus	Set temperature [K]	Char-N conversion (%)
Perching and Wendt [52]	Combustor		10–15
Spinti and Perching [51]	Combustor		40–60
Nelson et al [54]	EFR	1473	35–80*
Song et al [50]	EFR	1250–1750	20–35*
Molina et al [53]	EFR	1698	10–55
Phong-Anant et al [49]	EFR	1273–1873	30–50
Pohl et al [35]	EFR	1500	10–20*
Wang et al [60]	EFR	1273	10–45
Jensen et al [55]	Fixed bed	1123–1423	10–100

*** Only values of λ>1 are taken. Lower values were obtained when λ was <1**.

EFR: Entrained Flow Reactor (includes drop tube reactors).

As char-N conversion is closely linked to char conversion, a brief overview of char combustion is presented here. Char combustion can be divided into three zones based on which phenomena limits progression. In Zone I, the char conversion rate is kinetically controlled and increases rapidly with temperature. In Zone III, the conversion rate is controlled by the mass transport of oxygen to the char, which is less dependent upon the temperature. Zone II represents conditions in which both the kinetic and oxygen transport rates are important. High temperatures direct the combustion towards Zone III, since the chemical reaction rates increase, making mass transport the limiting factor. In contrast, the use of small particles directs the combustion towards Zone I, as the specific diffusive mass flux to the particle is increased, thereby promoting more rapid mass transport. High temperatures and small particles are present in pulverized coal combustion, and these systems are generally well represented by the conditions characteristic of Zone II [61]. Given the abovementioned factors, it is clear that it is complicated to describe char oxidation over a wide range of temperatures and combustion conditions, especially with respect to the partial pressure of oxygen. In general, neither global power-law kinetics nor semi-global Langmuir-Hinshelwood kinetics describe with sufficient accuracy the temperature-dependence. Instead, more complex models are required, some of which attempt to maintain dependence on just temperature and concentrations [62], while others include dimensionless numbers and specific coal parameters [63].

NO reduction

It is convenient to divide the NO reduction process during solid fuel combustion into reduction by volatiles and reduction by char, as these reactions occur on different time-scales. NO reduction by volatiles is important and is the main reason why air staging achieves significant reductions in NO levels, i.e., by prolonging the time in which NO can interact with the radicals formed by the volatile compounds. This mechanism is also used when fuel staging is applied, i.e., when introducing a fuel (e.g., natural gas) downstream of the initial combustion zone. The reduction of NO may occur through reactions with N-containing species (such as NH_i) or N-free species (such as CH_i) [64]. In those combustion systems in which fuel staging is not applied, NO reduction by volatiles only affects the NO that has been formed during the early stage of combustion, while the NO formed subsequently is not affected.

In contrast, the reduction of NO by char affects a larger fraction of the formed NO, since the char reactions occur on a longer time-scale. Many studies have been conducted on NO reduction by char and carbonaceous materials, several of which have observed a decrease in the apparent char-N-to-NO conversion as the background NO level is increased, i.e., the (NO_{out}-NO_{in})/char-N ratio decreases significantly as the initial NO concentration increases [51, 53, 57, 65]. Some of these studies have even observed negative rates of apparent conversion of char-N, i.e., more NO is reduced by the char than is formed by the char-N [51, 57]. This reduction appears to be enhanced in the presence of CO [58]. Aarna and Suuberg [66] have reviewed the studies on NO-char kinetics in the literature and averaged the rates; the resulting rate constant is shown in Figure 4 along with selected constants. Most of the rates found in the literature are within one order of magnitude of the Aarna and Suuberg rate. However, most of those studies have used chars that have been prepared prior to the experiments. Jensen et al [55] have shown that the rate of NO-char reduction decreases continuously in the time-span after pyrolysis, due to some deactivation mechanism, and that the rate directly after pyrolysis is significantly higher than that usually reported in studies in which the chars have been prepared separately. The rate reported by Song [67] is included in Figure 4, as it was obtained from experiments performed in the temperature range relevant to the conditions in a rotary kiln. The rate reported by Jensen et al [55], which is shown for comparison, is also applied in the modeling of this thesis. While it is significantly higher than the average rate provided by Aarna and Suuberg [66], it was derived in one of the few studies in which the char was produced *in situ* with the NO-char reactions proceeding directly afterwards. The rate described by Chan [68] was obtained at lower reactor temperatures. Nonetheless, it is recommended by Visona and Stanmore [58] for pulverized fuel combustion carried out at around 1750 K. Extrapolating this rate to higher temperatures results in a rate that is similar to that reported by Jensen and co-workers. Finally, it should be mentioned that Molina et al [57] increased by one order of magnitude the rate of Aarna and Suuberg to achieve fitting to their experimental data. This further indicates that the NO-char rate is higher than what is usually found in the literature, and that the rate reported by Jensen et al [66] is a strong candidate for describing the NO-char reduction in a PF flame.

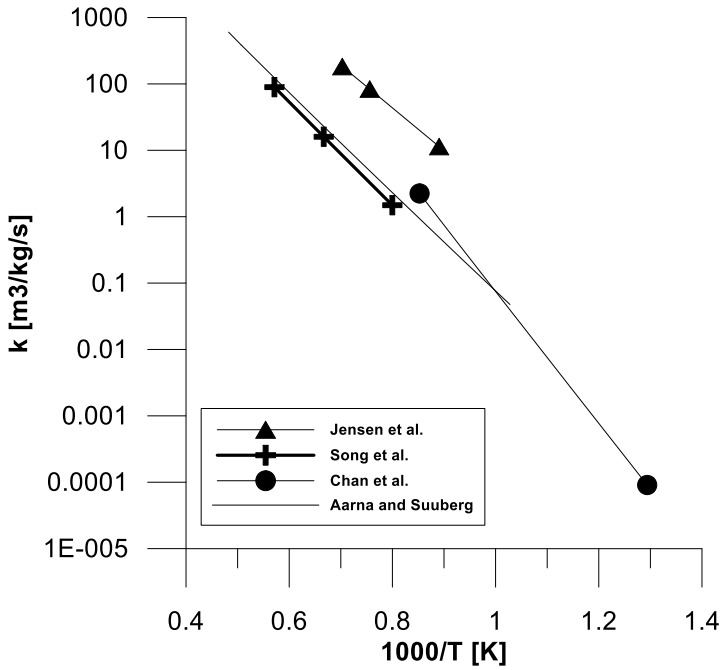

Figure 4. Arrhenius plot of the NO-char reaction. The reaction rates (in m^3/kg/s) are derived from Song et al. [67] and Aarna and Suuberg [66], assuming a char surface area of 150 m^2/g. An area of 530 m^2/g was used for the Chan rate [68]. As the reaction rate derived by Aarna and Suuberg [66] is an average rate, it does not include any symbols.

3.3 General NO_x mitigation strategies

Air staging

The most commonly used measure to reduce NO_x is to control the mixing of the air and the fuel to create an oxygen-lean zone during vol-N conversion, thereby yielding a lower rate of NO formation from volatile nitrogen. Mixtures that are overly oxygen-lean may, however, result in flame extinction. Burners are typically built with two registers for air: primary and secondary. The primary air may be premixed with the fuel or mixed rapidly. The secondary air is usually added through an outer register and is most often swirled, creating a reverse aerodynamic flow in the flame. Due to this reverse flow, hot (O_2-lean) gases are recirculated to the early part of the flame, which is beneficial for NO reduction. Swirling may also be applied to the primary air. There tends to be an optimal NO_x emission level with regard to swirling, as a low rate of swirling will not result in a significant recirculation zone, while a too-high rate of swirling will mix the air with the fuel too rapidly and NO_x formation will increase. Staging air through burner design is called 'internal staging'. It is also possible to stage the air externally by adding enough air through the burner to ignite the fuel, and adding the remainder at a later stage through separate ports (often called 'over fire air', OFA) (e.g., along the wall), to ensure burnout. For rotary kilns, OFA is not possible due to the rotation of the kiln.

Fuel staging

Introducing part of the total fuel input at a later stage in the combustor enables the formed NO to be reduced by, for example, hydrocarbon radicals (CH_i). The mechanism is called 'reburning', and it has proved to be an efficient way to reduce NO_x. The reburn fuel is typically natural gas, although solid fuels may also be used as long as they ignite readily and mix well. The reburn zone is generally sub-stoichiometric and additional air has to be added after this zone. Although fuel staging is generally performed externally, it is also possible to apply internal fuel staging using burners with different fuel registers.

Other primary measures

The relationship between stoichiometry and NO formation is clear; a lower stoichiometry (air/fuel) results in a lower level of NO formation, which means that decreasing the overall excess of air an effective measure. Although it is always the local stoichiometry that determines the level of fuel-N conversion, the global stoichiometry controls the ease with which local O_2-lean zones can be created. The stoichiometry in the early part of combustion can, as mentioned, be controlled effectively through burner design, whereas the stoichiometry in the later stages is less sensitive to such changes. However, decreasing the global stoichiometry lowers the O_2 levels post-flame inherently.

Another possibility is to recirculate the O_2-lean flue gases through the burner. This has three potential benefits for NO reduction: the reduction in O_2 concentration leads to decreased oxidation of fuel-N, as well as a lower temperature (reducing the thermal-NO mechanism), and the recirculation enables a reduction in the NO levels through reburning. Substantial reductions in NO levels have been attained in oil- and gas-fired boilers owing to the decrease in thermal-NO formation, while this strategy has proven to be less effective for solid fuels [69].

Fuel switch

Since fuel-N is a significant contributor to NO formation in PF flames, a simple measure that is often used is to switch to a fuel that contains less nitrogen. Switching from a solid fuel to a gaseous fuel tends to decrease significantly the NO_x emissions. However, the linkage between the fuel-N content in solid fuels and NO emissions is weak, as fuel-N conversion depends on many other aspects. Thus, changing to a solid fuel with a lower nitrogen content does not guarantee a lower level of NO_x formation. The content of volatiles has, for example, been shown to play a significant role. In unstaged flames, a higher volatile content leads to higher NO emissions, whereas for staged flames the opposite trend is observed. The reason for this is that a fuel that has a high content of volatiles is likely to release more volatile nitrogen, and if air staging is achieved it will affect a larger fraction of the total fuel-bound nitrogen. Other fuel properties, such as particle size and ash content, can also play important roles, so it is difficult to predict the effect on NO of a fuel swap.

Another possibility is to co-combust the fuels. Apart from reducing the amount of incoming fuel-N, the interaction between the two fuels has the potential to create NO reduction by forming additional, local O_2-deficient zones. In theory, a volatile fuel with low nitrogen content could be manipulated so that a reducing zone is formed at an optimum location, thereby reducing the fuel-N conversion from the other fuel [70]. Co-combustion also facilitates the combustion of certain fuels that may be difficult to ignite. Using a small amount of gaseous fuel can, for example, stabilize a solid fuel flame.

Secondary measures

If NO_x emissions cannot be reduced effectively using primary measures, flue gas cleaning may be necessary. This is performed by adding ammonia (NH_3), which reacts with NO to form N_2. Urea [$CO(NH_2)_2$] is also used, since it decomposes to NH_3 but is safer to handle. The reaction between NO and NH_3 is highly temperature-dependent, and it is most efficient at temperatures in the range of 900°-1100°C. At higher temperatures, the oxidation of ammonia becomes more prominent, which can result in increased NO emissions, while at lower temperatures, the reaction may not proceed to completion and ammonia may be emitted (so-called ‘ammonia slip’).

The reduction of NO by NH_3 is possible at lower temperatures (200°-500°C) if a catalyst is present. This is selective catalytic reduction (SCR), and it can provide significant NO_x reduction. The reduction without a catalyst is called selective non-catalytic reduction (SNCR) and is less common in industrial systems.

3.4 Scaling

In raw material-producing industries, such as the iron and steel industry, having strong production flows and high utilization rates is crucial to the business, such that any modifications to the processes are carefully evaluated using a scaling procedure prior to full-scale implementation. However, scaling is a difficult task as it influences almost all combustion aspects. The International Flame Research Foundation (IFRF) states that “*the scaling of combustion systems with complete similarity is practically impossible*” [71]. It is, therefore, important to be aware of the effects that scaling can have on the combustion process.

The two most common ways of scaling PF combustion processes are constant velocity scaling and constant residence time scaling. To understand these criteria, it is helpful to write the inlet velocity (u_0) as follows:

$$u_0 = \frac{V_0}{A} = \frac{4V_0}{D_0^2\pi} = \frac{4m_0}{\rho_0 D_0^2\pi} \quad \text{Eq. 2}$$

where, typically, V_0 and m_0 are the volumetric and mass flow rates of combustion air through the burner, A is the cross-section area of the burner, ρ_0 is the density of the combustion air, and D_0 is the diameter of the burner throat. For rotary kiln systems, it is however not straight-forward to define which air flows and diameter should be used for the calculations, as will be shown in Chapter 5.1. If we want to relate the air mass flow to the fuel input, we can expand m_0 as:

$$m_0 = M_{air}\lambda N_{0,stoich} m_{fuel} \quad \text{Eq. 3}$$

where M_{air} is the molar mass of air, λ is the air-to-fuel equivalence ratio, $N_{0,stoich}$ is the stoichiometric amount of air required to achieve complete combustion of the fuel (in $kmol_{air}/kg_{fuel}$), and m_{fuel} is the mass flow of fuel. If we also include that the fuel heat input (Q) is equal to the mass flow of fuel (m_{fuel}) times the heating value of the fuel (H_i), we obtain:

$$u_0 = \frac{4M_{air}\lambda N_{0,stoich} Q}{D_0^2 \rho_0 \pi H_i} \quad \text{Eq. 4}$$

When scaling a combustion process, usually only a few of these values change, and it is, therefore, common to simplify the equation as:

$$Q = K\rho_0 u_0 D_0^2 \quad \text{Eq. 5}$$

where K represents the values that do not change during scaling. If constant velocity scaling is applied, u_0 is kept constant while Q and D_0 are varied. If constant residence time scaling is applied, the value of D_0/u_0 is kept constant. For constant velocity scaling, the relation between D_0 and Q becomes:

$$D_0 \propto Q^{0,5}$$

and for constant residence time scaling:

$$D_0 \propto Q^{0,33}$$

For example, if the fuel input is scaled by a factor of 64, the diameter of the down-scaled burner should be scaled by a factor of 8 if constant velocity scaling is applied, and by a factor of 4 if constant residence time scaling is applied.

According to Smart et al [72], both scaling criteria should maintain the factional degree of mixing over the normalized axial length x/D_0. This means that both scaling criteria should achieve satisfactory outcomes if the combustion reactions are sufficiently rapid for the combustion to be fully controlled by mixing. This could, in theory, be applicable to gaseous fuels, since there is no inherent mass transfer resistance to limit the progress of combustion. However, even for gaseous flames, scaling is difficult, as demonstrated in the Scaling 400 project conducted by the IFRF (see for example Hsieh et al [73] and Weber [74]). For liquid and solid fuels, the two-phase interactions complicate the process even more. A 40-kW oxy-coal burner was successfully scaled up to 80 kW by the application of a constant residence time-scale, as described by Toporov [75]. However, echoing the IFRF statement, Toporov has written that "*direct scale-up of the burner described above to an industrial scale oxy-firing burner in the range of several MWth, however, is not possible*".

The recent work by Weber and Mancini [76] provides RANS simulations of five flames in the range of 0.176–50.0 MW, revealing how constant velocity scaling affects the flame characteristics. In the low thermal input range, the particles penetrate deeper into the internal

recirculation zone (IRZ), which means that the devolatilization occurs in a fuel-rich environment, while in the high thermal input range devolatilization occurs mainly in the air stream. The authors mention that when scaled to even lower thermal inputs (40–80 kW), flame blow-off occurred. Constant velocity scaling for PF-flames is, therefore, not guaranteed to be successful. While constant residence time scaling is in theory a superior scaling method, it is rarely applied in practice owing to problems related to the reduced velocity in small scale [71].

3.5 Units of emission measurements

Several units for quantifying NO_x emissions are used depending on the application. A common unit used in research is the volumetric gas fraction of NO_x (in ppm), as it is the unit that is employed by most measurement instruments. The volumetric gas fraction is equivalent to the molar gas fraction and proportional to the partial pressure and concentration (mol/cm^3). The latter is, however, dependent upon system conditions such as pressure and temperature.

Neither of these units directly quantifies the amount of NO_x formed in the process, as they both depend on the flue gas flow and the values are decreased if the gas is diluted. A common approach to account for dilution is to correct the NO_x fraction to a certain base oxygen level. This correction is performed according to:

$$x_{NO_x,corrected} = x_{NO_x} * \frac{x_{O_2,ox} - x_{O_2,base}}{x_{O_2,ox} - x_{O_2}} \quad \text{Eq. 6}$$

where $x_{NO_x,corrected}$ is the corrected molar NO_x fraction, x_{NO_x} is the measured molar NO_x fraction, x_{O_2} is the measured molar O_2 fraction, $x_{O_2,ox}$ is the oxygen molar fraction in the oxidizer (≈0.21 for air), and $x_{O_2,base}$ is the base oxygen fraction to which the emission should be corrected (0.06 for solid fuels within the EU).

It is also common to use the unit mg_{NO2}/m^3_n instead of the molar fraction. This unit is equivalent to the molar fraction, and the conversion is obtained by applying the ideal gas law and assuming that all the NO is converted to NO_2. Correction to a base oxygen level might still be necessary, and it is also performed using Eq. 6. It may also be of interest to look at the ratio of emitted NO_x to introduced fuel-N, since this relates to the performance of the combustion process with regard to NO_x emission. NO_x emissions corrected to 6% O_2 and the NO_x to fuel-N ratio are used mainly in **Papers I** and **II**.

Another common practice is to relate the emitted NO_x to the energy input, i.e., mg_{NO2}/MJ. An advantage of using this unit system is that it relies on the actual amount of NO_x in the flue gases. It does, however, require accurate measurements of the flue gas flow and the fuel feed, which are not always available. Attention must also be paid to the specific heating value (lower or higher) on which the unit is based. This unit is used primarily in **Papers III** and **IV**.

For the Grate-Kiln process, use of the molar fraction or mg_{NO2}/m^3_n corrected to a certain oxygen level should be avoided, as the product (the pellets) absorb a certain amount of oxygen, thereby introducing an error when one attempts to correct the NO_x measurement. Nonetheless, this approach is used throughout this thesis as there were no pellets present in the pilot-scale kiln experiments and to facilitate comparisons with other units and regulation limits. When presenting NO_x emissions from the full-scale plant as values corrected to an oxygen concentration, the NO_x emission is first calculated as mg_{NO2}/MJ_{fuel} and then converted[1] to ppm and corrected to 6% O_2.

[1] See Appendix A for how this conversion is performed.

In **Paper IV**, the unit NO_x/CO_2 is applied because it is used in the reports that the paper reviews. NO_x/CO_2 is an uncommon unit and not suitable for comparing NO_x emissions from different fuels. However, if the burnout is complete, it generates an easily-obtained normalized value that gives a good indication of whether a primary measure manages to reduce NO_x emissions or not.

A unit that is commonly used in industrial production processes is NO_x/unit of production. In the Grate-Kiln process, this is expressed as g_{NO2}/tonne pellets, and it may be advantageous because it incorporates the production efficiency of the plant. It is, however, difficult to compare NO_x emissions across industries using this unit system.

Units that are corrected to a certain oxygen level or related to the energy input are often used in legislation aimed at industrial applications. The review of Baukal and Eleazer [77] provides more details on this. Finally, it should be noted that these units indicate the environmental performances of individual plants, and that using them in designing legislation incentivizes the use of BAT. The environmental impact on a regional or global level is, however, more sensitive to the absolute amount of NO_x emitted than to the concentrations in flue gases. For example, for evaluating the degree of pollution, kg_{NO2}/year is superior to mg_{NO2}/m^3_n. The Gothenburg protocol and EC Directive 2016/2284/EU use units of $kton_{NO2}$/year.

4 Previous work on NO_x formation in rotary kilns

Rotary kilns are efficient for high-temperature heat treatment of solid material. In addition to iron ore manufacturing, typical applications include cement production, lime manufacturing, lightweight aggregate manufacturing, reduction of oxide ore, and waste incineration [78]. As the most common application of rotary kilns is cement production, research on combustion in kilns has focused on that application. This section provides an overview of the previous findings regarding NO_x formation in cement and iron ore kilns. It should be noted that there are significant differences in kiln design and usage between industries: sintering cement clinker may require a bed temperature as high as 1540°C and the flue gas oxygen concentration is in the range of 1%–4% [79, 80], whereas iron ore is sintered at around 1250°C and employs a level of excess air that is equivalent to 15%–17% oxygen in the flue gases [81, 82].

4.1 Cement industry

The specific NO_x emissions from cement kilns that fire solid fuels are in the range of 1300–2500 g/tonne clinker, while for gaseous fuels the corresponding level can be three times as high [83]. In China, 10% of the NO_x emissions originate from the cement industry [84] (with reference to [85]). The BAT document for cement production [86] states that as a yearly average, the outlet NO_x concentration from European cement kilns is about 380 ppm, with a minimum of 70 ppm and a maximum of 990 ppm (all corrected to an oxygen level of 10%). In many cement production plants, NO_x reduction by primary measures is carried out either in the kiln or in the calciner, which the flue gases enter after the kiln. Intensive efforts have been made to reduce the levels of NO_x in the calciner, and a NO_x reduction of up to 60% has been achieved through calciner modifications [26]. Among the various studies of NO_x control in cement manufacturing, there is a consensus that thermal NO formation dominates NO formation in the rotary kiln. Strong evidence for this is the fact that flame cooling through the injection of water is an efficient way to reduce NO_x emissions [87].

Vaccaro [88] has reviewed NO_x campaigns performed in industrial cement kilns, largely based on the CEMFLAME project by the IFRF and a research program conducted by the European Commission, both in the 1990s [89, 90]. The review concludes that significant NO_x reductions could be achieved through the use of low-NO_x burners. In kiln systems, these burners have two primary air inlets (one is swirling and one is axial) and one fuel inlet. The amount of primary air used was considered to be especially important. The NO_x emission levels could be reduced by 45% (compared to a mono-channel burner) by reducing the amount of primary air while maintaining stable operation. In a review performed by McQueen et al [83], decreasing the level of primary air was shown to have the potential to reduce NO_x levels by 30%. Other primary measures were found to contribute NO_x reductions in the range of 15%–30%, while the use of SNCR and SCR could reduce NO_x levels by 40%–70% and 70%–90%, respectively.

Both the European Union and the US Environmental Protection Agency have published documents on NO_x control in the cement industry that include several proposed measures [91, 92]. Reducing the amount of excess air (i.e., reducing the flue gas oxygen concentration from 2% to 1%) was shown to decrease the levels of NO_x by 15%. An innovative strategy that has been proposed for dealing with NO_x is fuel staging by means of "mid-kiln firing", which entails the use of a fuel inlet through the wall half-way along the rotary kiln. This allows for slow-burning fuels, such as whole tires, to be introduced once per rotation of the kiln. Since the energy input of the kiln inlet can be reduced by this measure, the combustion is dispersed, and the level of NO_x is reduced by as much as 50%. The use of low-NO_x burners does not always yield reductions in NO_x, although reductions of up to 35% have been reported.

4.2 Iron ore industry

The specific NO_x emissions from iron ore kilns firing solid fuels are typically in the range of 150–400 g/tonne of pellets, and become about three-times higher when natural gas combustion is applied [28]. The BAT document for iron and steel production [93] shows that the NO_x emissions for three pelletization plants are in the range of 36–138 ppm, although it is unclear if these values are corrected to a specific oxygen concentration. If the oxygen concentration is 17%, which is a typical stack oxygen concentration in Grate-Kiln plants, the above ranges becomes 99–380 ppm when corrected to an oxygen level of 10%, i.e., slightly lower than the NO_x emissions of cement plants. However, as stated in Chapter 3.5, correction to an oxygen content is not the optimal method for measuring NO_x emissions in iron ore induration plants.

Very little research has been performed on the emissions performances of iron ore rotary kilns, and many aspects are assumed in the literature to be shared with cement rotary kilns. In iron ore rotary kilns, firing with natural gas has been shown (as in cement kilns) to produce more NO_x than firing with solid fuels [28], which underlines the importance of thermal NO formation. Similar to cement kilns, the high levels of NO_x emissions produced during solid fuel combustion are assumed to result from the dominance of thermal NO formation. As will be discussed in Chapter 7, this thesis questions this assumption and suggests that fuel-N is the dominant source of NO_X emissions from the iron ore rotary kiln.

The modeling of a gas-fired rotary kiln for iron ore production performed by Davis [94] revealed a minimum level of NO formation at a certain secondary air flow. A too-low level of secondary air flow resulted in a high level of NO formation due to the long residence times and high peak temperature (i.e., high thermal NO formation), while a high secondary air flow resulted in high-level NO formation due to the increased O_2 levels, although the temperatures were reduced. Apart from this study and some general reports on emissions [28, 93, 95], not much research has been done or is available on NO_x in rotary kilns for iron ore production.

5 Experimental

This chapter describes the experimental setup used for the work described in this thesis. The first part describes the design and dimensions of the combustion facilities, along with calculations of the inlet velocities and convective mixing times. The second part describes the measurement equipment that was used.

Several fuels have been tested and evaluated. The bituminous coal, denoted as 'Coal A' in this work, is in focus in **Papers I–IV**, as it is used in the daily operation of the LKAB plants. In **Paper V**, a different bituminous coal, called 'Sufco', is combusted. The fuel analyses for these two coals are presented in Table 2. For the fuel analyses of the remaining fuels see **Paper IV**.

Table 2. Fuel analyses of Coal A used in **Papers I–IV** and of the Sufco coal used in **Paper V**.

	H_2O	**Ash**	**VM**	**C**	**H**	**N**	**O**	**LHV**
unit	%-wet	%-wet	%-wet	%-dry	%-dry	%-dry	%-dry	MJ/kg
Coal A	0.9	13.1	21.4	76.1	3.9	1.4	5.1	29.4
Sufco	6.53	12.8	38.3	67.6	4.7	1.2	13.7	24.8

VM, volatile matter; LHV, Lower Heating Value.

5.1 Combustion facilities

Experimental data from four combustion facilities have been used in this work: a full-scale iron ore rotary kiln; a pilot-scale kiln; and two pilot-scale combustors, called L1500 and OFC (oxy-fuel combustor). **Papers I–IV** are based on data from the pilot-scale kiln and of these, **Papers III** and **IV** provide comparisons with the full-scale kiln. The L1500 and the OFC combustors are used in **Paper V**.

When discussing rotary kilns along with conventional furnaces, it is important to define the nomenclature. In most combustion facilities, primary air is defined as the air injected through the same burner register as the fuel (i.e., as transport gas), and secondary air is the air that enters through other registers, e.g., swirl air. In rotary kilns, primary air is defined as all the air that is introduced through the burner (including swirl or axial air), and secondary air is introduced externally to the burner through two inlets located above and below the burner. Figure 5 shows the definitions used in discussing combustion in kilns and in the present work.

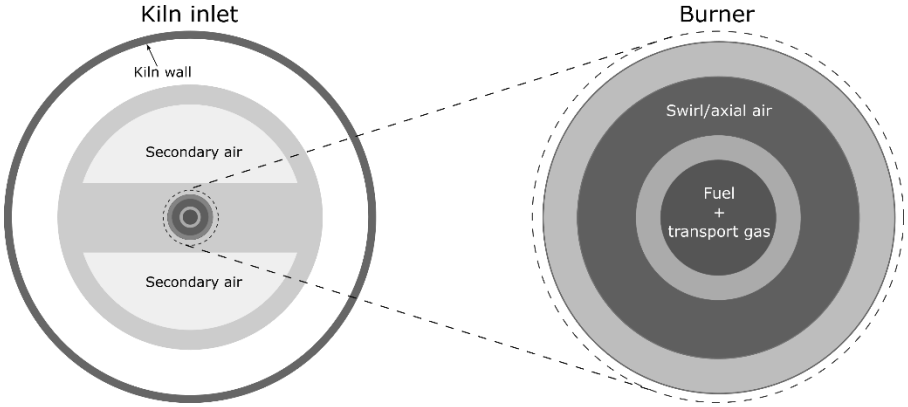

Figure 5. Schematic of a kiln inlet and burner orifice, showing where the air flows are injected. In kilns, the air flow through the burner is defined as 'primary air' and may be divided into transport, axial and swirl air. The 'secondary air' is the air that enters the kiln separate from the burner. In conventional burners, like the L1500 and the OFC, the transport air is defined as the 'primary air' and the other air flows are 'secondary air'.

The full-scale kiln

The full-scale reference kiln is used in the LKAB KK2 plant, located in Kiruna, Sweden. The KK2 plant produces around 4 million tonnes of iron ore pellets annually and has been in operation since 1981 [81]. The kiln is inclined at an angle of 4° so that the pellets gradually move forward under force of gravity. The kiln is rotating at 1.4 rpm to ensure that the pellets are thoroughly mixed. The iron ore pellets form a rolling bed at the bottom of the kiln, taking up about 10% of the kiln volume. The fuel is usually a bituminous coal, and the fuel heat rate is about 40 MW, depending on the pellet production rate. The secondary air is preheated to >1000°C by the processed hot pellets in the cooler. No secondary measures for NO_x reduction are implemented at the plant.

Figure 6 shows a photograph of the burner in the full-scale kiln. The burner, which has a central position within the kiln, consists of a central pipe through which the coal is fed along with transport air. Two annular swirl registers surround the coal pipe. The diameter of the coal pipe is 85 mm, and the outer diameters are 138 mm and 160 mm for the inner and outer swirl registers, respectively. The outer swirl register is, however, not in use.

Figure 6. Photograph of the burner used in the LKAB KK2 plant. Solid fuel and transport air are injected through the central pipe, and swirl air through the inner swirl register. The outer swirl register is not in use.

The pilot-scale kiln

The LKAB pilot-scale kiln is a downscaled version of the KK2 kiln and is used for fuel and burner evaluations. Two versions of the pilot-scale kiln are evaluated in this work: The Year 2013 kiln, with a heat input of 400 kW_{fuel}; and the Year 2015 kiln**,** with a heat input of 580 kW_{fuel}. The following description is of the Year 2015 kiln since it has been used for most of the experiments and modeling in this thesis (**Papers I–IV)**. Only in **Paper IV** has the Year 2013 kiln been evaluated.

The Year 2015 kiln is scaled down using constant velocity scaling. The length of the kiln is 14 m, and the diameter is 650 mm for the first 4.4 m, after which the diameter expands to 800 mm. Only the first 4.4 m section is considered to be the kiln. The reason for extending the furnace to 14 m is mainly to be able to perform, for example, slagging measurements. The rotation of the kiln is not included in the pilot-scale setup. The kiln is equipped with both horizontally and vertically arranged access ports for in-flame measurements of temperature, concentrations, radiation, and heat flux. The kiln also includes a cooling system at the bottom part of the kiln, to simulate the heat sink of pellets.

Secondary air at a temperature of 1000°C–1100°C enters through two channels located above and below the centrally positioned burner. The burner (Figure 7) has six registers: two for

primary air, and four for fuel. One primary air register is swirled (N4), while the other register introduces air axially (N1). Different fuel registers may be used depending on which full-scale plant is being simulated by the pilot-scale setup. In **Paper I**, the central fuel register (N6) was the most frequently used, as the goal was usually to replicate the KK2 conditions. This register had a diameter of 12.5 mm and register N5 had a diameter of 22.5 mm. The transport gas for these registers was N_2. The swirl register (N4) consisted of 24 small holes on a disc with an outer diameter of 35 mm. Register N3 had an outer diameter of 58 mm and register N2 had an outer dimeter of 73 mm. The axial register (N6) consisted of 36 small holes on a disc with an outer diameter of 85 mm. When co-combusting coal and biomass, coal was fed through N3 and biomass was fed through N2, to simulate the conditions of another LKAB plant located in Svappavaara, Sweden.

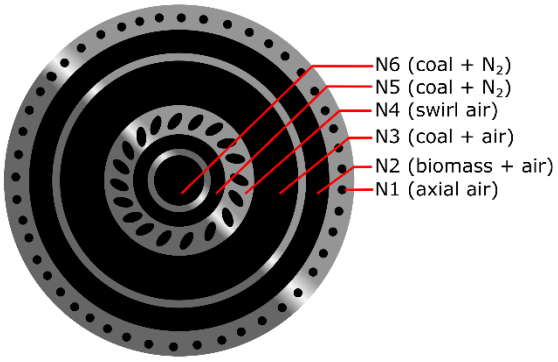

Figure 7. Illustration of the frontal view of the pilot-scale kiln burner showing all six fuel and air registers.

The Oxy-Fuel Combustor

The oxy-fuel combustor (OFC) is a vertical, down-fired combustor, with an inner diameter of 0.61 m in the combustion zone, located at the University of Utah, Salt Lake City, UT, USA. While the OFC is designed for inputs of up to 100 kW, in the experiments performed in **Paper V**, it was fired at a fuel input of 30 kW. The outlet oxygen concentration was maintained at 3%-dry.

A co-axial burner with central coal-feeding and an outer annulus for secondary air was used. The coal pipe had a diameter of 12 mm, while the secondary air register had an inner diameter of 27 mm and an outer diameter of 41 mm. A register designed for gas combustion was located between the two registers but was not used in this work. This burner creates a jet flame (Type-0).

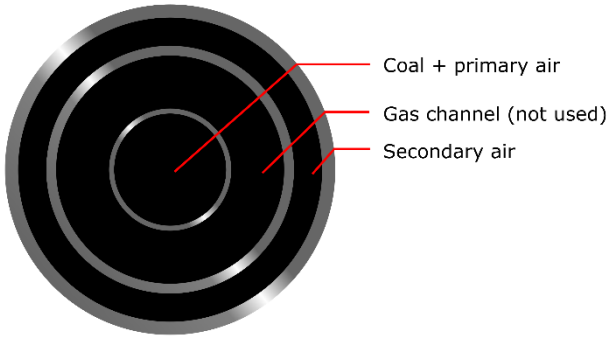

Figure 8. Illustration of the burner orifice for the burner used in the oxy-fuel combustor. Only the central pipe and the outer registers were in use for the work in **Paper V**.

The L1500 furnace

The L1500 is a horizontal furnace located at the University of Utah, Salt Lake City, UT, USA. The combustor has a length of about 12 m and the square cross-section has a width of about 1 m. There are several measurement ports located along the length of the furnace.

Figure 9 presents the co-axial annular burner with an adjustable swirl setting, as used in **Paper V**. Coal and primary air were fed through the central annulus, which had a diameter of 76 mm. Three annular registers surrounded the central coal pipe, of which the innermost register was designed for gas firing and was not in use. The outer two registers were used for secondary air and had outer diameters of 154 mm and 203 mm. Two types of flames were produced in this combustor: a swirled flame with a swirl angle of 75° (applied to both secondary air registers), and a jet flame without any swirl. For both flames, the burner operated under sub-stoichiometric conditions ($\lambda = 0.8$), and over-fire air (OFA) was injected at an axial distance of about 4 m to complete burnout. The fuel input was 1 MW, and the outlet oxygen content was 3%-dry.

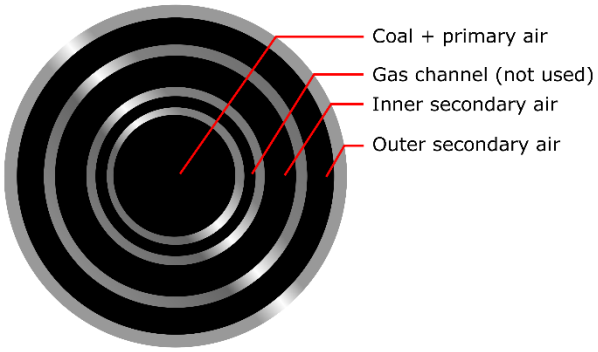

Figure 9. Illustration of the burner orifice of the burner used in the L1500 furnace in **Paper V**.

Comparison of combustion facilities

The test facilities used are summarized and compared in Table 3. It's worth to mention that an effort was made to scale the combustion process only between the full-scale kiln and the pilot-scale kiln. To relate the facilities to each other, the u_0 values are calculated using Eq. 4. However, the definition of the diameter, D_0 in Eq. 4, is difficult to establish for kilns, as a large fraction of the air is introduced outside the burner. A considerable part, albeit not all, of this air will be entrained into the flame and influence the velocities in the flame. The share and position of the entrainment of secondary air into the flame are two important aspects. Thus, three u_0 values are presented, based on the diameters of the central coal pipe, the burner throat (based on register N4 for the pilot-scale kiln), and the entire furnace, respectively. The calculations based on the furnace diameter are not of significant interest for the L1500 and the OFC, as these are enclosed combustion chambers and do not include the secondary air flows like the kiln systems. Therefore, these values are given in parentheses.

The pilot-scale kin, the full-scale kiln, and the OFC show high values for u_0 when calculated based on the coal pipe, which is expected for jet flames. The velocities in the full-scale kiln and pilot-scale kiln are of similar magnitude, independent on which value of D_0 that is used, indicating that constant velocity scaling has been successfully applied. The convective mixing time (D_0/u_0) is, however, significantly shorter in the pilot-scale than in the full-scale, indicating that mixing occurs faster in the pilot-scale setup.

Table 3. Comparison of the characteristics of the combustion facilities used in this thesis. The values inside parentheses for the L1500 and the OFC are calculated but not of special interest, since they have confined combustion chambers.

		Full-scale kiln	Pilot-scale kiln	OFC	L1500
Q_{fuel} [MW]		40	0.58	0.03	1
$L_{furnace}$ [m]		34	4.4	1.2	14
$D_{coal\ pipe}$ [m]		0.085	0.0125	0.012	0.076
D_{burner} [m]		0.14	0.03	0.041	0.2
$D_{furnace}$ [m]		5	0.65	0.61	1
$\lambda_{coal\ pipe}$ [-]		0.012	0.019*	0.32	0.24
λ_{burner} [-]		0.04	0.11	1.16	0.8
$\lambda_{furnace}$ [-]		4	4	1.16	1.16
u_0 [m/s]	Coal pipe	24.0	25.5	24.1	14.9
	Burner	27	26	11.6	6.8
	Furnace	10.7	9.1	(0.03)	(0.42)
D_0/u_0 [ms]	Coal pipe	3.5	0.49	0.5	5
	Burner	5.3	1.15	5.5	29.5
	Furnace	468	71	(18,040)	(2,384)

* Assuming that air instead of N_2 is used as the carrier gas.

The flat-flame burner

A flat-flame burner was used in **Paper IV** to estimate the level of nitrogen partitioning during pyrolysis. A low rate of coal feeding (about 1 g/h) was used to ensure single-particle behavior. A stream of N_2 was used as the carrier gas and the particles were injected about 1 mm above the FFB surface. The average temperature was 1392°C, and the average residence time was 1.33×10^{-2} s, i.e., the particles were warmed rapidly with a heating rate of approximately 10^5 °C/s. The char samples were then collected and sent for analysis.

5.2 In-flame measurements

Characterization of a PF flame is challenging due to the high spatial and temporal gradients. During in-flame measurements, data are collected at each measurement position for a certain amount of time (several minutes), to derive a representative average. Several data-points are required to map the flame spread. Furthermore, fluctuations in the fuel feed and difficulties associated with attaining steady-state conditions, for example constant wall temperatures (which may affect the flame), are issues that are commonly encountered in pilot-scale facilities that are not run continuously.

Another challenge is to measure a property at a certain point while minimally disturbing the flame. The most common forms of in-flame measurements are *intrusive*, i.e., a probe is inserted at the desired location and measures a property, either directly or by extracting gas or particles to be analyzed in an external instrument. These probes are cooled to withstand the high

temperatures of the flame. Both the cooling and the volume of the probe will, of course, affect the flame temperature and flow field around the measurement position. The extent to which the flame is affected is, however, difficult to establish. Ideally, one wants to perform measurements that are *non-intrusive*, for example using new optical techniques. These techniques typically involve transmitting a laser beam that interacts with the flame characteristic of interest and measuring the resulting radiation with detectors. Although there are many advantages and possibilities associated with such techniques, they require adequate optical access, and the laser beam may affect the flame being characterized. The lasers themselves can also be large and require several fine adjustments, and it may be inconvenient to move them to, for example, another measurement port. Therefore, in terms of mobility and flexibility, intrusive measurements are more convenient. Nevertheless, there are optical measurement techniques that are portable and easy to use, e.g., infrared (IR) cameras.

Temperature measurements

Temperature measurements are typically performed with thermocouples, which produce a temperature-dependent voltage from which the temperature can be derived. Figure 10 gives an illustration of the thermocouple and probe used for in-flame measurements. To ensure that the thermocouple is heated to the temperature of the flame, it needs to be shielded with a ceramic shell, as the furnace wall temperatures are lower than the flame temperatures and would otherwise exert a significant radiative cooling effect on the thermocouple. The shielding also protects the thermocouple from physical damage by particles. Furthermore, the gas velocity around the thermocouple should be around 200 m/s, to achieve sufficient convective heat transfer. Increased gas velocity is achieved by applying suction around the thermocouple. A drawback of the suction is that the volume of gas that is sucked out of the flame makes the measurement less of a point measurement.

For the measurements performed in **Papers I** and **V**, a triple-shielded thermocouple of type B (suitable for temperatures <1800°C) was mounted on a cooled probe with suction. The probe was traversed across the flame. Approximately 4 minutes were required for the thermocouple to stabilize at each measurement point. Figure 10 shows a schematic of the suction pyrometer, as well as a photograph of the ceramic shield after an in-flame measurement.

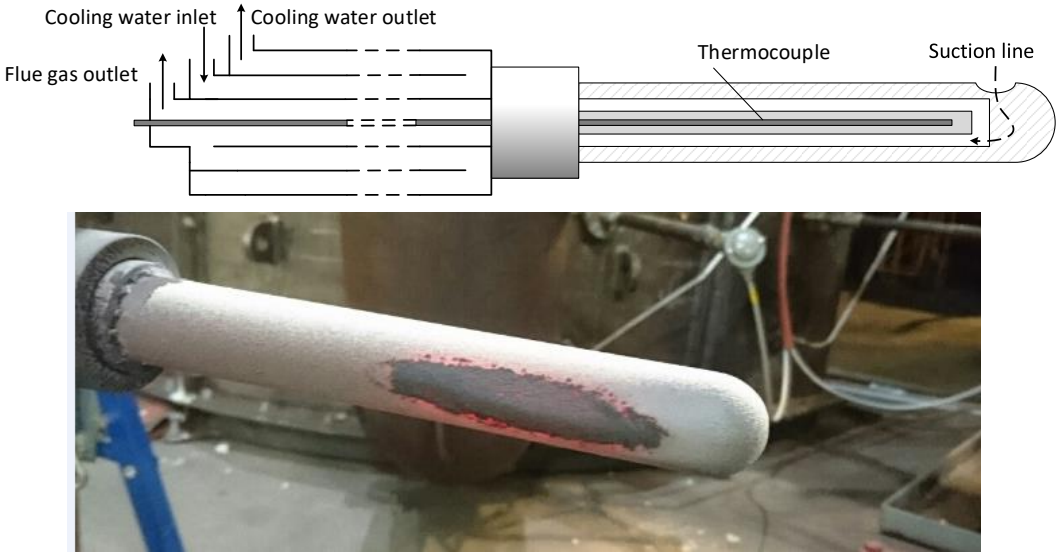

Figure 10. Top panel: Schematic of the suction pyrometer. Courtesy of Adrian Gunnarsson [96]. Bottom panel: Photograph of the protective ceramic around the thermocouple after measurement. As the gas inlet is on the other side, it is not visible in this image. Hot coal particles adhere to the ceramic shield after the measurements.

Gas composition measurements

There are several ways to measure the concentration of a specific gas in a gas mixture. A common approach is to force the gas mixture through a cell and direct light of a set wavelength, commonly infrared (IR) or ultraviolet (UV), through the cell in the direction of a detector. If the gas mixture contains a gas that absorbs light of the set wavelength this will be detected by the detector and the extent of attenuation of the light can be used to determine the actual concentration of the gas. A standard IR gas analyzer typically measures 1–3 gases simultaneously.

A technology that effectively measures more gases simultaneously is Fourier-Transform Infrared (FTIR) spectroscopy, which scans a wide range of wavelengths in the IR spectrum. Instead of using a light source that has only one wavelength (monochromatic), FTIR spectroscopy uses a light source with multiple wavelengths (polychromatic). The light from this source enters a so-called Michelson interferometer (Figure 11) where the light beam is split into two beams: one is refracted to a fixed mirror, while the other is refracted to a moving mirror. The beams are reflected back to the beam splitter, where destructive and constructive interference phenomena occur depending on whether the wavelengths are in phase, which in turn is dependent upon the distances between the mirrors and the beam splitter. The resulting beam enters a sample cell that is filled with the gas mixture, where absorption of certain wavelengths occurs depending on the gases present in the mixture. The remaining beam is measured with a detector. Since one of the mirrors is moving, different distances between the mirror and beam splitter are created, so that different wavelengths experience constructive/destructive interference, and this means that the light entering the sample cell varies. The result is a so-called ‘interferogram’, which is transformed into a spectrum using the Fast Fourier Transform. A computer then compares this spectrum with a reference spectrum (typically, an N_2 spectrum) and analyzes which wavelengths have been absorbed and to what extent. Knowing which wavelengths are relevant for which gases, it calculates the concentration of each gas. An issue with FTIR gas analyzers is that although every gas can be associated with a unique set of absorption wavelengths, a gas may share individual wavelengths with other gases, which may result in an error. For example, if gas A absorbs wavelengths x and y, which are also absorbed by gases B and C, it may appear that gas A is present even though only gases B and C are present. Therefore, it is necessary to have an inkling as to which gases could be present in the mixture. Another drawback is that FTIR spectrometers do not detect symmetrical diatomic gases (e.g., O_2), since these molecules lack a dipole moment and, therefore, will not interact with the electric field of the light. In the case of O_2 measurements, it is possible to use a paramagnetic instrument that relies on the magnetic property of O_2.

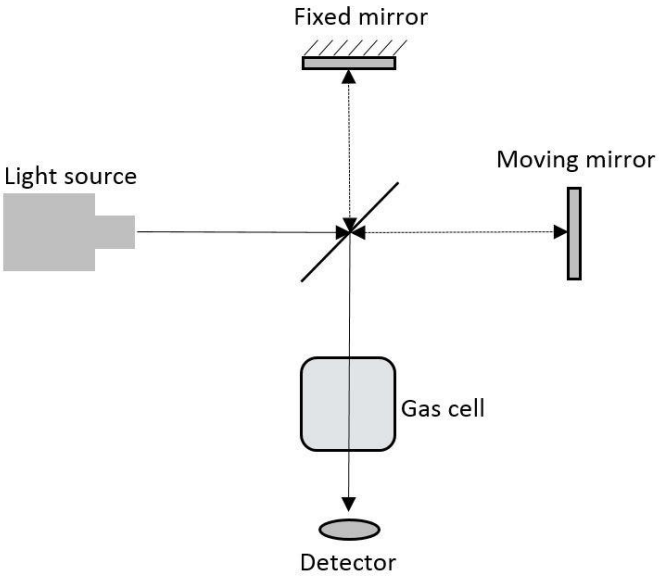

Figure 11. Schematic of the Michaelson interferometer, which is a central component of FTIR spectroscopy.

For the gas concentration measurements performed in **Papers I** and **V**, the in-flame gases were extracted by suction probes and analyzed using FTIR spectroscopy for CO_2, H_2O, CO, HCl, HF, N_2O, NH_3, NO, NO_2, SO_2 and HNO_3, and using paramagnetism for O_2. The gas was passed through a filter, to protect the measurement equipment from particles, and was then led through an electrically heated tube (≈190°C), to avoid condensation. The gas was assumed to experience instantaneous quenching. A schematic of the probe tip and a photograph of the probe tip before measurements are presented in Figure 12. A potential problem with these measurements is clogging of the filter by particles, which may cause unwanted heterogeneous reactions when the gas is suctioned through the filter. This can also cause unwanted pressure drops in the measurement equipment.

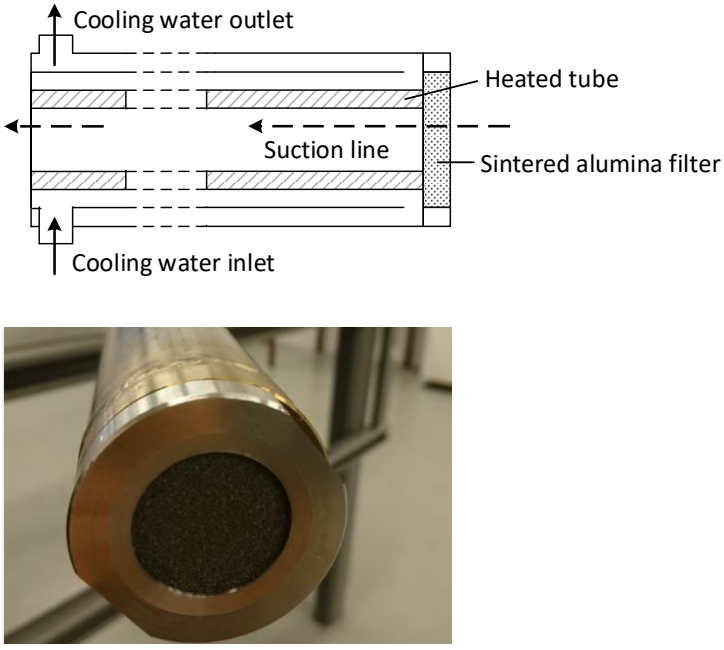

Figure 12. Top panel: Schematic side-view of the gas probe. Courtesy of Adrian Gunnarsson [96]. Bottom panel: Frontal view of the gas probe before any measurements were performed.

In-flame measurements in this work

Figure 13 shows where in-flame measurements of temperature and gas composition were made for each combustion unit in this work. The measurement ports are indicated by dotted lines. The axial distance of each facility is normalized with regard to the diameter of the coal pipe of the burner (see Table 3 for these values) for easier comparison. There are no in-flame measurement possibilities in the full-scale kiln. For the pilot-scale kiln and the OFC, in-flame measurements are performed in similar locations with an extra early measurement for the pilot-scale kiln. The L1500 has a shorter normalized length than the other facilities, which makes sense because the L1500 coal pipe is significantly larger and does not create a jet flame.

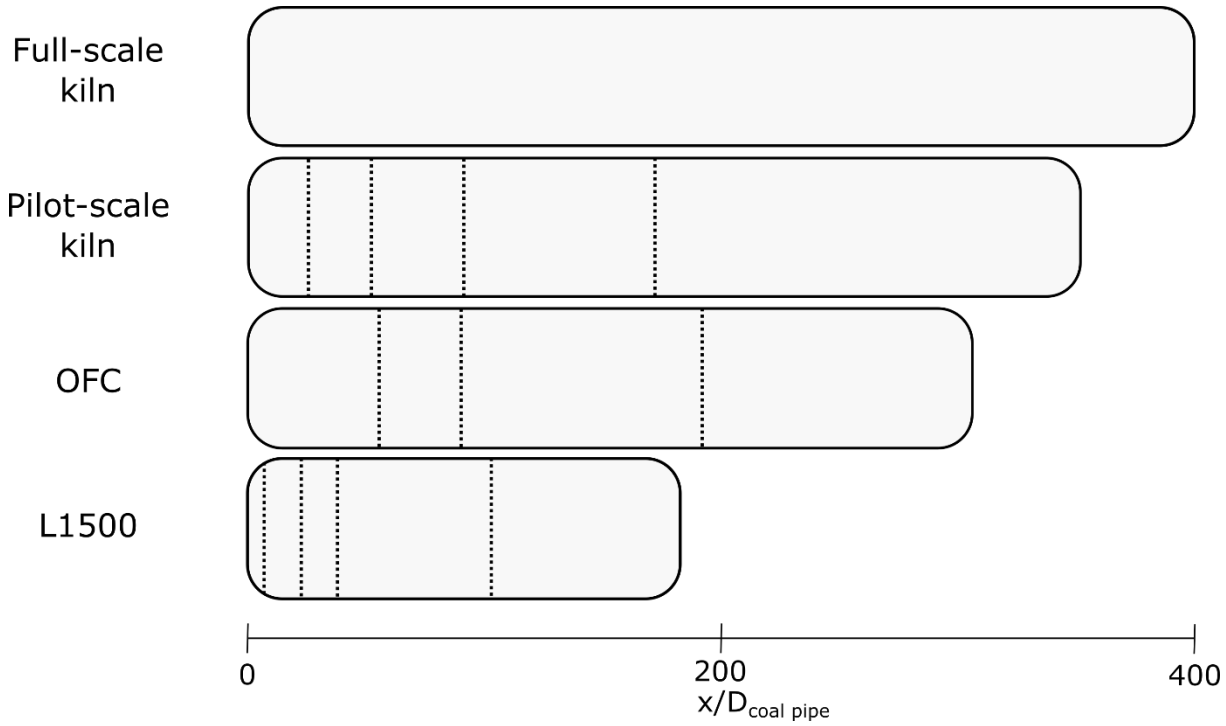

Figure 13. Visual comparison of the combustion facilities with the axial distance normalized to the diameter of the burner coal pipe in respective facility. The coal pipe diameters are 0.085m, 0.0125m, 0.012m and 0.076m for the full-scale, pilot-scale, OFC and L1500 respectively. The dotted lines indicate where in-flame measurements of temperature and gas composition were made.

6 Modeling

When using modeling to describe a phenomenon that occurs during a complex process, such as solid fuel combustion, it is highly challenging to decide on what to include and exclude in the model. A common dilemma when modeling combustion is that while both the aerodynamics and the reaction rates are of great importance, describing both of these simultaneously is problematic. One reason for this is the computational power required for detailed descriptions of both aspects. Another reason is that the interactions of all combustion phenomena are not well understood and trying to introduce as many aspects as possible will inevitably introduce uncertainties and result in errors. Modeling using Computational Fluid Dynamics (CFD) typically relies on detailed descriptions of the flow fields and the mixing processes but uses less-detailed descriptions of reaction rates. In contrast, detailed reaction modeling relies on simplified approaches to describe mixing but includes detailed reaction schemes. In this work, a detailed reaction model is used.

6.1 Model description

Figure 14 presents a schematic overview of the model. The model describes the combustion chemistry and NO formation during the combustion of a fuel. In theory, it can be used as a predictive model. However, for this, the model would require information on heat losses, to calculate the temperature profile, as well as an estimation of the mixing profile between the fuel and oxidizer. Instead, providing the model with a temperature profile (from, for example, measurements) and fitting the mixing profile to existing O_2 and CO measurements avoids these uncertainties and provides a detailed description of the combustion conditions in a given process. Analyses of the reaction pathways and the governing reaction mechanisms may then be performed. Table 4 presents an overview of how the model treats the characteristics of combustion, such as the kinetics, mixing, heat release, heat transfer, species concentrations, temperature, and fuel, all of which are important and interconnected.

Kinetics and mixing

The in-flame combustion chemistry is investigated using a plug flow reactor (PFR) model. The fuel is injected at the inlet of the PFR and the air is introduced in a staged manner, i.e., the fuel stream is gradually diluted with air. This process represents the mixing of fuel and air. The air is divided into primary air and secondary air, with the primary air being mixed with the fuel at a higher rate. The mixing rate is dependent upon the total flow of air and the share of the flow introduced at a given distance within the PFR (defined by the user). The mixing rate is high if a lot of air has been injected at a short distance in the PFR. A longer injection distance equals a slower mixing rate. The combustion chemistry is described by the detailed reaction kinetics proposed by Mendiara and Glarborg [97] for the homogeneous reactions, and the apparent kinetics are described by Jensen [98] for the heterogeneous reactions. The detailed homogeneous reaction mechanism involves 97 species and 779 reactions. In addition, the following irreversible heterogeneous reactions with apparent kinetics are included: (i) the conversion of char into CO (R1); (ii) the oxidation of char-N to NO (R2); and (iii) the reduction of NO by char (R3 and R4). The reduction of NO by char is described by two reactions. Table 5 presents the reactions and the corresponding kinetics.

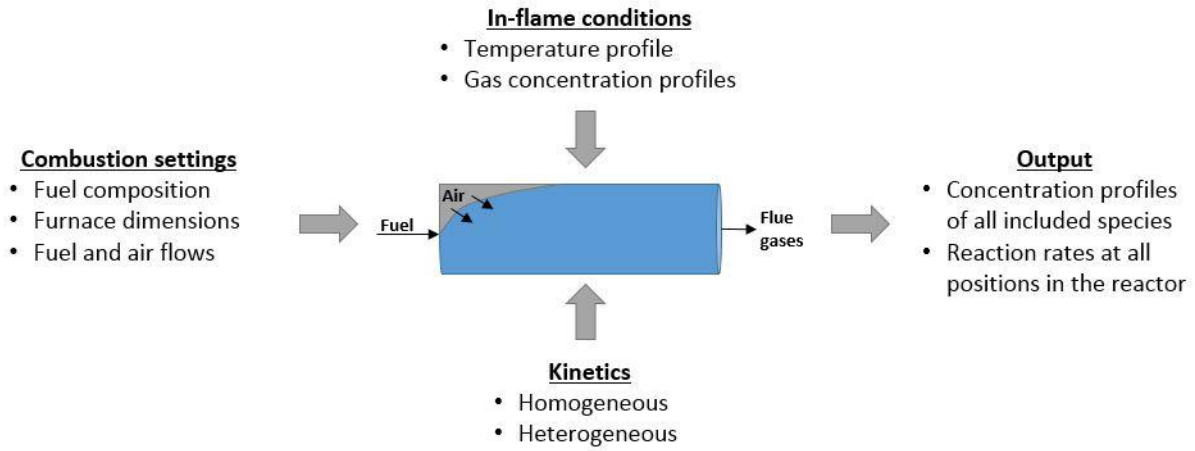

Figure 14. Illustration of the model structure, showing the inputs and outputs.

Table 4. Summary of the ways in which combustion characteristics are treated in the modeling.

Combustion characteristic(s)	Treatment in the modeling
Kinetics	• Detailed homogeneous reaction kinetics are used for the volatiles • Apparent kinetics are used for the heterogeneous kinetics
Mixing	• Mixing is defined by how rapidly air is added to the fuel in the axial direction • Mixing on a smaller scale (e.g., through eddies and vortexes) is not considered
Heat release, heat transfer, and temperature	• The energy equation is not solved. Instead, the temperature profile is given as an input from measurements (or CFD)
Fuel composition	• The volatiles are assumed to consist of CH_4, CO, H_2 and HCN • Char and Char-N are modeled as $C_2(s)$ and $N_2(s)$ that are converted only through irreversible heterogeneous oxidation • Ash is treated as a fully inert component • Water is assumed to be in the form of vapor from the start
Ignition and pyrolysis	• Ignition is inherently controlled by the kinetics and depends on the temperature and gas composition • The pyrolysis is assumed to be instantaneous • Tars are neglected
Particle characteristics	• Properties related to the solid particles, such as porosity, surface area, fragmenting, and swelling, are ignored

Table 5. Reactions and kinetics of the heterogeneous mechanism.

	Reaction	A [cm³/mol/s]	E_a [cal/mol]
R1	$C_2(s) + O_2(g) \rightarrow 2\ CO\ (g)$	2.24×10^{11}	29,400
R2	$N_2(s) + O_2(g) \rightarrow 2\ NO\ (g)$	2.24×10^{11}	29,400
R3	$NO(g) + C_2(s) \rightarrow CO(g) + CN(s)$*	1.46×10^{11}	29,400
R4	$2\ CN(s) \rightarrow C_2(s) + N_2(g)$*	$1.00E\times10^{20}$	0

*The overall reaction of $NO(g) + ½\ C_2(s) \rightarrow ½\ N_2(g) + CO(g)$ is implemented as a two-step reaction, with R3 as the controlling step.

This mechanism assumes full conversion of char-N to NO. Thus, the reduction of NO by char dictates the apparent conversion. In the original heterogeneous mechanism proposed by Jensen [98], the conversion of char-N to NO was 75% (25% conversion to N_2), based on observed values of 50%–100% under single-particle conditions for temperatures in the range of 850°–1150°C. However, it was only at 850°C that the char-N-to-NO conversion did not reach 100% under single-particle conditions [55]. Since the operating temperatures during char combustion in iron ore rotary kilns will be even higher, 100% conversion of char-N to NO is applied in the present work.

Fuel properties

The contents of volatiles, moisture, and ash, as well as the elemental composition of the fuel are given as inputs to the model. Moisture in the fuel is modeled as water vapor, i.e., the impact of vaporization is not included, and the ash is modeled as an inert component that does not interact with the combustion process. The char is represented as $C_2(s)$, and the volatiles are assumed to consist of CH_4, H_2, and CO. The split between the volatile components is determined by the elemental balances for C, H, and O:

$$Y_{CO}\left(\frac{M_C}{M_{CO}}\right) + Y_{CH_4}\left(\frac{M_C}{M_{CH_4}}\right) = \frac{X_{C,fuel} - X_{char}}{1 - X_{char}} \quad \text{Eq. 7}$$

$$Y_{H_2}\left(\frac{2M_H}{M_{H_2}}\right) + Y_{CH_4}\left(\frac{4M_H}{M_{CH_4}}\right) = \frac{X_{H,fuel}}{1 - X_{char}} \quad \text{Eq. 8}$$

$$Y_{CO}\left(\frac{M_O}{M_{CO}}\right) = \frac{X_{O,fuel}}{1 - X_{char}} \quad \text{Eq. 9}$$

where Y_i is the mass fraction of species *i* in the volatiles, M_i is the molar mass of species *i*, and X_k is the fuel mass fraction of element *k* in the fuel (dry, ash-free basis). The system of equations is then solved to obtain the value of *Y* for CH_4, H_2, and CO. This is a simplification of the approach proposed by Thunman et al [99].

The nitrogen content of the fuel is split between the volatiles and char, i.e., a share is released with the volatiles as HCN, while the remainder is released with the char as '$N_2(s)$'. This share is set by the user. Table 6 gives an example of the composition of the modeled and actual fuel composition assuming that vol-N and char-N have 50/50 shares and using Eqs. 3–5. In **Paper IV**, the char yield results from the flat-flame burner were used as input to the model in the form of X_{char} (instead of the proximate analysis). The nitrogen content in the char was also used to determine the nitrogen partitioning (rather than simply assuming it).

Table 6. Fuel composition of Coal A used in the pilot-scale kiln and the corresponding modeled fuel composition (assuming a 50/50 split between vol-N and char-N). The composition is given on a wet basis.

Actual composition	Unit	Value	***Modeled composition***	Unit	Value
Fixed carbon*	mass-%	64.6	**C_2 (s)**	mass-%	63.9
Ash	mass-%	13.1	**Ash**	mass-%	13.1
H_2O	mass-%	0.9	**H_2O (g)**	mass-%	0.9
Volatiles	mass-%	21.4	**CO (g)**	mass-%	8.2
C	mass-%	75.4	**CH_4 (g)**	mass-%	11.1
H	mass-%	3.9	**H_2 (g)**	mass-%	0.79
O	mass-%	5.9	**HCN (g)**	mass-%	1.32
N	mass-%	1.37	**N_2 (s)**	mass-%	0.68
O_2-demand	m^3_n/kg_{fuel}	1.59	**O_2-demand**	m^3_n/kg_{fuel}	1.58

*Calculated by difference (100-Volatiles-Ash-H_2O).

Reaction analysis

The Chemkin solver calculates the rates of all the reactions at each step in the PFR using the law of mass action:

$$rate = k \prod c_i^{\nu_i} \qquad \text{Eq. 10}$$

where k is the rate constant (see Eq. 1), c_i is the concentration of the i^{th} reactant in the reaction, and $\nu^{\,i}$ is the stoichiometric coefficient for the i^{th} reactant. Reverse reactions are calculated through the use of thermodynamic data. The resulting rate at each step in the PFR is given in $mole/cm^3/s$. Since the purpose of the model is to evaluate NO formation during combustion, each rate is integrated, either over volume or residence time, in order to evaluate its overall importance. The net formation of NO (in mol/s) in the PFR is derived by integrating the net NO formation rate over the volume of the reactor. Likewise, the level of NO production from char-N and the level of NO reduction by char are calculated by integrating R2 and R3, respectively. The thermal formation of NO is usually described by R3-2–R3-4. However, due to the fact that the reverse reaction of R3-2 and the forward reaction of R3-4 are central to the net conversion of vol-N to NO, these reactions cannot simply be integrated to obtain the thermal NO formation. In **Paper II**, only the forward reactions of R3-2 and R3-3 are considered to be part of the thermal NO formation mechanism.

To compare NO formation between combustion systems at different scales, the formation of NO is divided by the fuel input (in MW_{fuel}). The resulting value is then in units of mol_{NO}/MJ_{fuel}. This can then be converted to e.g. mg_{NO2}/MJ_{fuel}.

6.2 Modeling NO formation

To illustrate how NO formation via the thermal NO mechanism and the conversion of volatile nitrogen are affected by temperature and local stoichiometry (mixing rate) in the model, a sensitivity analysis is provided in Figure 15–17. The simulations are performed using an isothermal PFR with a length of 5 m. The gas velocity is set at 5 m/s so that the residence time is 1 s in all the simulations. In Figure 15a, only air is present in the reactor. In Figure 15b, air

is introduced at the inlet and fuel (CH_4) is rapidly injected at 200 cm (injection is finished at 210 cm). In Figure 15c, CH_4 is introduced at the inlet and air is rapidly injected at 200 cm. The flow rates are 10 g/s for air and 0.57 g/s for the fuel.

From Figure 15a at 1600°C, the NO level increases exponentially with the reactor length. This is due to the initially slow production of O radicals from the thermal dissociation of O_2. The O radicals react with N_2 and form NO and N radicals. The N radicals can then react with O_2 to form NO and new O radicals. Once the thermal mechanism gains momentum, O radicals are produced from O_2 both by dissociation and by reaction with N radicals. For temperatures <1600°C, however, scarcely any NO is formed. In Figure 15b, which represents the same case but with CH_4 injected at 200 cm, NO formation is increased significantly at all temperatures. This can be explained by the increased availability of both OH and O radicals from the chain-branching reaction which is enabled by the introduction of CH_4. Similar results are shown in Figure 15c, although it also shows that when air is added to the fuel, the lower local stoichiometry leads to a lower rate of NO formation.

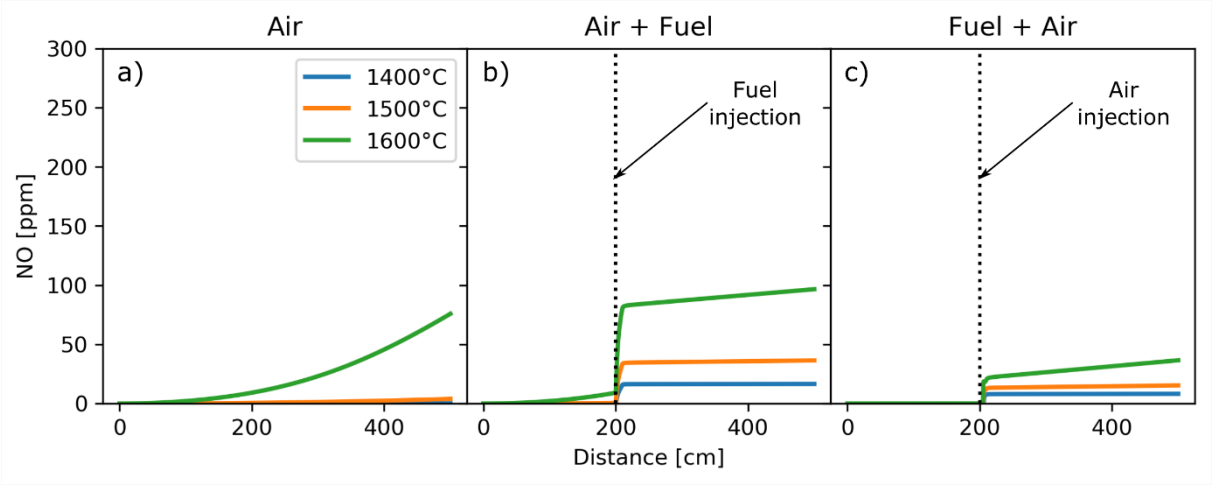

Figure 15. NO formation profiles in an isothermal PFR, showing the influences of temperature and mixing on thermal NO. The cases depicted are: a) plug flow of air; b) plug flow of air with rapid CH_4 injection; and c) plug flow of CH_4 with rapid air injection.

In Figure 16, the same simulations are performed as shown in the previous figures, albeit with the addition of 1 mg/s HCN. In Figure 16a, HCN is premixed with the air, while in Figure 16, b and c, it is considered part of the fuel (i.e., the fuel is CH_4 plus HCN). The figures show that the addition of HCN increases the NO formed by a similar amount (about 100 ppm) in all cases, except for the premixed case (i.e., case a) where the NO concentration increases more linearly than previously. This is because the small amount of HCN contributes to an increase in O radicals early in the process, whereas in Figure 16a, O radicals had to be first formed from the thermal decomposition of oxygen. The slope of the NO profile is steeper in Figure 16a than in Figure 16, b and c due to the higher O_2 concentration.

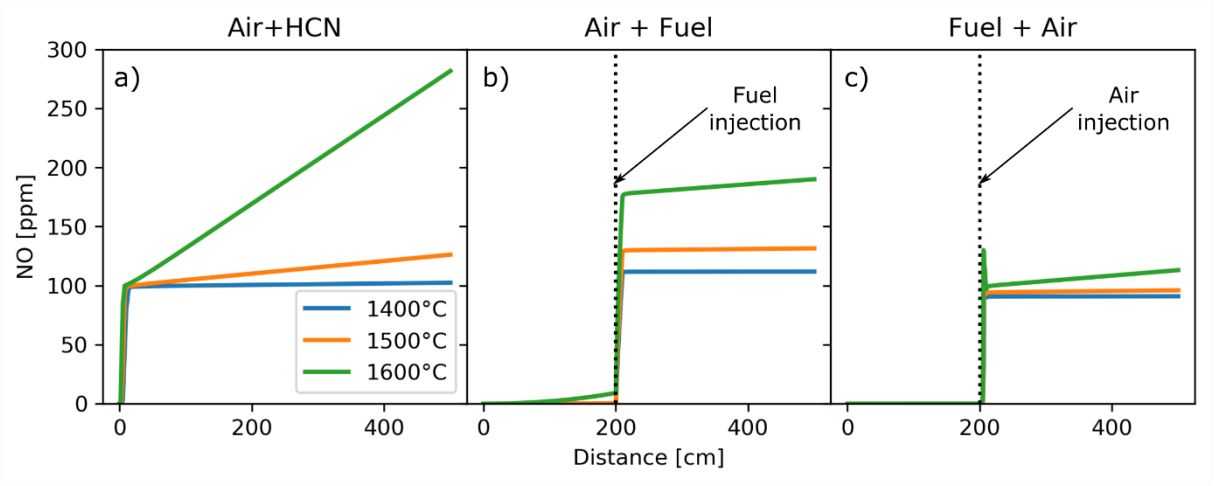

Figure 16. NO formation profiles in an isothermal PFR, showing the influences of temperature and mixing on NO formation when HCN is present. The cases depicted are: a) plug flow of air plus HCN; b) plug flow of air with rapid CH_4 plus HCN injection; and c) plug flow of CH_4 plus HCN with rapid air injection.

In Figure 15b-c and Figure 16b-c, the mixing of the fuel and air occurred rapidly. In Figure 17, the mixing rate is reduced (continuous injection between 200 cm and 400 cm). When fuel is added to the air (Figure 17a), NO formation is higher than when the mixing is fast (Figure 16b), and the formation rate is sensitive to the temperature. When air is injected into the fuel (Figure 17b), the NO concentrations are about half the concentrations noted when the injection is rapid (Figure 16c), and the formation of NO appears to be less sensitive to the temperature. These graphs illustrate the importance of local stoichiometry. In Figure 17a, the air-to-fuel equivalence ratio increases from 0 to 1.02, while in Figure 17, it goes from infinity to 1.02. This means that the local conditions are oxygen-rich for a significant amount of time in a) but are oxygen-lean in b). In Figure 16, the time spent at an air-to-fuel equivalence ratio above or below 1.02 is significantly shorter.

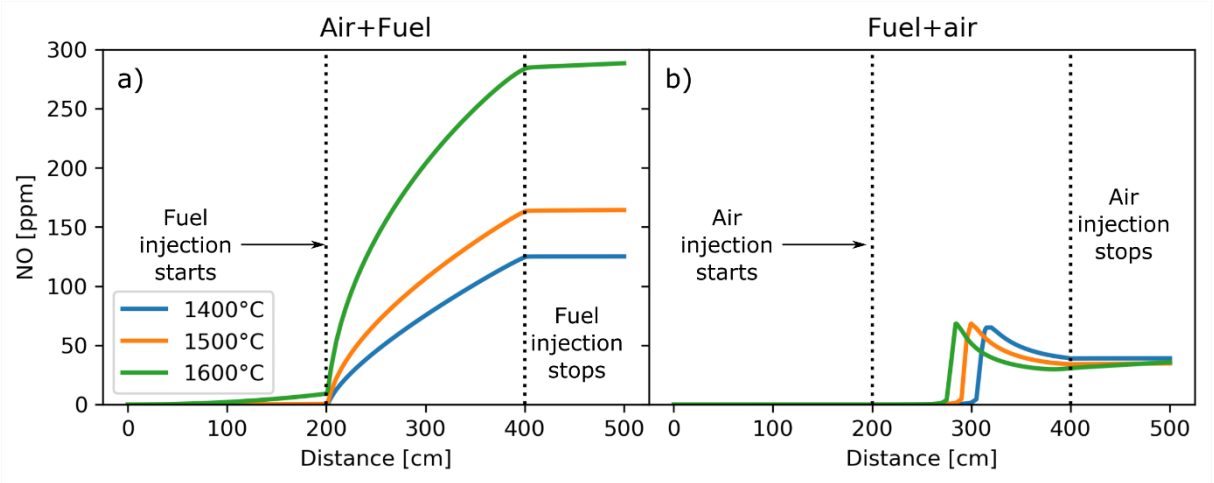

Figure 17. NO formation profiles in an isothermal PFR showing the influences of temperature and mixing on NO formation. The cases shown are: a) plug flow of air with slow CH_4 plus HCN injection; and b) plug flow of CH_4 plus HCN with slow injection of air.

Figure 15–17 show that the NO formation from gaseous reactions is heavily dependent upon the local conditions. A turbulent diffusion flame consists of several zones with different local temperatures, gas compositions, and stoichiometries, and the residence times in these zones vary. When a solid fuel such as coal or biomass is combusted, heterogeneous reactions add to this complexity.

7 Results and Discussion

This chapter summarizes the most important results from the appended papers in relation to the research topics of this thesis.

7.1 NO formation routes

In-flame measurements from **Paper I** were used as input to the model in **Papers II** and **III** to investigate the contributions of homogeneous and heterogeneous reactions to total NO formation. The simulations of the pilot-scale kiln showed that the partitioning of the fuel-nitrogen is crucial. In general, the NO formation from the vol-N was low, but the combustion conditions during char combustion contributed significantly to NO formation. Since the apparent conversion of char-N to NO is primarily dependent upon the reduction of NO by char, it means that the reduction of NO by char was inefficient. The amount of NO_x formed through the thermal NO mechanism was of low importance. When the amount of primary air was increased, vol-N contributed significantly more.

In **Paper III**, the effects of scaling were investigated by applying the same (normalized) temperature and mixing profiles in the pilot-scale and full-scale kilns. The results for NO formation are shown in Figure 18. The model captures the reduced level of NO formation in the full-scale (which was observed experimentally) and attributes it to a lower NO contribution from the heterogeneous reactions, i.e. a more efficient reduction of NO by char in full-scale. This turns out to be the combined effect of the constant velocity scaling and the rate of char conversion. Since the velocities are the same in both kilns, but the full-scale kiln is significantly longer, the fuel residence time under oxygen-lean conditions becomes longer in full-scale. In contrast, the fuel stream penetrates further into the pilot-scale kiln where more oxygen is available. As a consequence, char is oxidized faster by O_2 and the reduction of NO becomes less efficient. If the combustion would have been entirely controlled by mixing, this would not be an issue, but since the char consumes O_2 slower than the rate of which O_2 is becoming available, the char experiences a more oxidizing atmosphere in the pilot-scale kiln. The contribution from homogeneous reactions, i.e. vol-N conversion and thermal NO formation, are however well preserved during the scaling process.

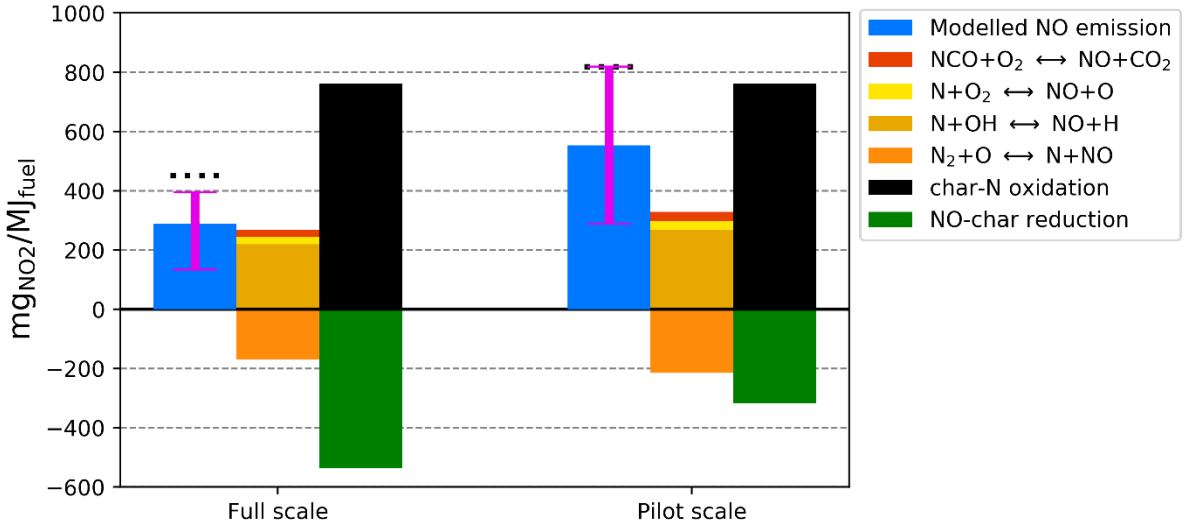

Figure 18. Bar diagram showing the levels of NO formation normalized to the fuel input in the full-scale and pilot-scale as calculated by the model using a vol-N:char-N ratio of 1:1. The first bar represents the total NO formation, the second bar is the formation of NO from the homogeneous reactions, and the third bar represents the NO formation from the heterogeneous reactions. The dotted lines represent the measured emissions. The error bars are for vol-N:char-N ratios of 1:3 (upper error bar) and 3:1 (lower error bar), respectively.

The simulations performed in **Papers II** and **III**[2] were performed such that air was mixed into a stream of fuel, similar to what was performed in the experiments described in Figure 17b, i.e., combustion starts under sub-stoichiometric conditions and then gradually attains the global stoichiometry. As shown in the modeling section, this approach leads to less thermal NO formation than if the fuel is injected into a stream of air. Figure 19 presents modeling results from when CH_4 is injected into an air stream, representing a 'worst case scenario' where the conditions for thermal NO formation are optimized. This result is presented along with the measured and calculated NO profiles in **Paper II**. The temperature profile (based on measurements[3]) was the same in both simulations as well as the exit concentration of O_2. A third case with CH_4 injection into an air stream but with the temperature profile increased by 100°C at all points is also provided. Even with an increase of 100°C at all positions and favorable mixing conditions, thermal NO formation is low compared to the NO formed from the fuel-bound nitrogen.

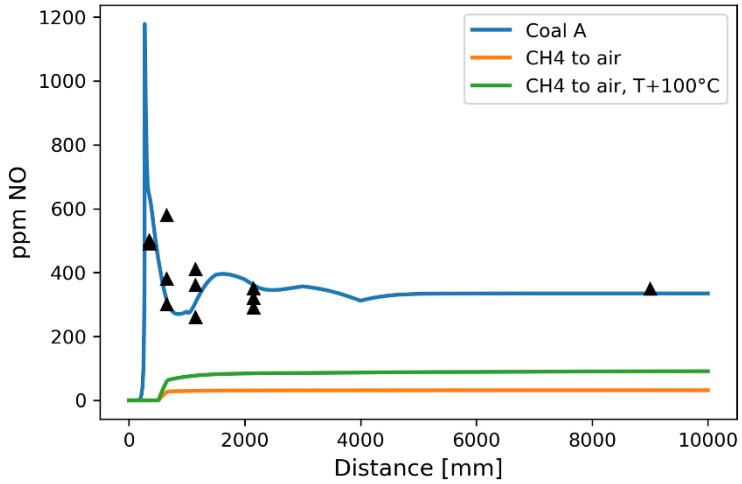

Figure 19. NO profiles for three modelled cases. In-flame measurements of temperature as well as O_2 and CO concentration are used for the temperature and injection profiles (based on Coal A combustion). Coal A: Fuel is described by the model according to the fuel analysis of Coal A. CH4 to air: Same simulation as Coal A but with methane instead of Coal A (same stoichiometry). CH4 to air, T+100°C: Same simulation as 'CH4 to air' but with the entire temperature profile increased by 100°C. Symbols: measurement points.

From the results in **Paper I-III** it is established that char-N dominates the NO formation in iron ore rotary kilns. The apparent conversion of char-N to NO is the result of O_2 and NO competing for char sites, and the concentration ratio $[O_2]/[NO]$ during char conversion is thus a controlling factor. The high level of excess air entrainment into the flame leads to a high O_2 concentration and also results in a low NO concentration due to dilution by N_2. This knowledge should be kept in mind when attempting to reduce NO_x formation in iron ore rotary kilns.

7.2 The impact of fuel type on NO_x emissions

Figure 20 shows the measured levels of NO_x emissions from the solid fuel experiments in the pilot-scale kiln (**Paper I**) and in the full-scale kiln (**Paper III**). For comparison, data from other, mostly unstaged, flame studies taken from the literature [52, 74, 90, 100] are included as gray symbols. The limit stated in the Medium Combustion Plant Directive (MCPD) [101] by the EU is also included as a reference to what a 'low' level of NO_x infers. Some important observations from this graph are that: (i) the levels of emissions are clearly higher from the pilot-scale kiln

[2]See Appendix B for a discussion of the differences between the mixing profiles used in **Paper II** and **Paper III**.

[3]See Appendix C for temperature measurements of the Coal A flames obtained in **Paper I**

than from the full-scale kiln; and (ii) although the NO_x emissions are high from the full-scale flames relative to, for example the MCPD limit, they are not remarkably higher than NO_x emissions from several other flames studies found in literature. In pilot-scale, a general trend between the levels of emissions and the fuel nitrogen content can be detected. The cases with the lowest nitrogen contents (N-content ≈ 0.85%) are the co-firing cases with coal and biomass. In these flames, the substitution of 30% coal with biomass reduced the ingoing nitrogen level by 25% and reduced the NO_x emissions by 23%. However, it is clear from the range of emission levels that parameters other than nitrogen content are also important for NO_x formation. The lowest NO_x emissions in the pilot-scale kiln are achieved with modified burner settings for Coal A (N-content = 1.38%), and the fuel with the highest nitrogen content (N-content = 2.35%) does not produce the highest NO_x emissions.

The measured level of NO_x emissions from when gas and oil were combusted are shown in Table 7. Gas was not fired in the full-scale kiln, and the oil and gas combustion in the pilot-scale kiln were conducted in an older version of the kiln (described in **Paper IV**) without a cooling system to represent the pellets. Nevertheless, these results show that the combustion of oil or natural gas can lead to more than twice the level of NO_x emissions compared to when firing solid fuels, as observed in the pilot-scale kiln. For these fuels, thermal NO is naturally the main formation mechanism (the nitrogen content in the oil was 0.23%) and these results indicate that thermal NO can potentially be an issue in iron ore kilns. However, the level of NO_x emission can also become lower than when firing solid fuels due to the reduced amount of fuel-bound nitrogen, as observed in the full-scale kiln.

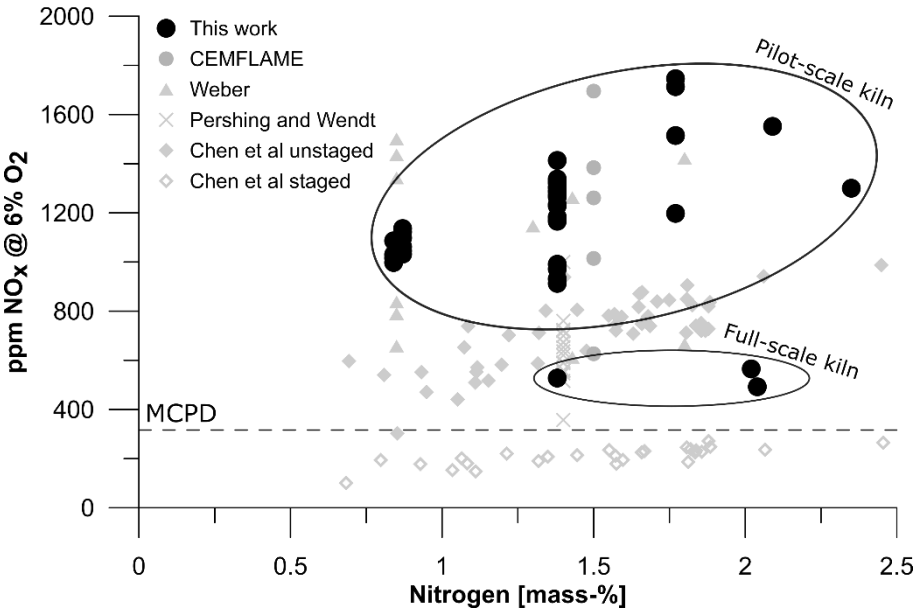

Figure 20. NO_x emissions from the combustion of solid fuels in the pilot-scale kiln experiments described in **Paper I** and from the full-scale kiln described in **Paper III**. The tests conducted with a nitrogen content of 0.85% N represent co-firing flames with coal and biomass. For comparison, NO_x emission data from the literature are presented as gray symbols and the Medium Combustion Plant Directive (MCPD) as the dashed line.

Table 7. NO_x emissions from firing the pilot-scale and full-scale kilns with oil and natural gas (in ppm corrected to 6% O_2).

	Pilot-scale	**Full-scale**
Oil	2665	410
Natural gas	2565	N/A

7.3 The impact of burner settings on NO_x emissions

The term 'burner setting' refers here to the configuration of primary air flows (transport, swirl and axial air) through the burner and the fuel registers that are in use. In **Paper I**, it was found that the total amount of primary air was more important to the NO formation than the individual effects of transport, swirl or axial air. The influence of total primary air on NO_x formation in the pilot-scale kiln is presented in Figure 21 in terms of burner stoichiometry. There is a correlation between the amount of formed NO_x and the amount of primary air for the cases when the fuel is fed through the fuel registers inside the swirl register, i.e. N6 or N5. When the fuel is fed through the annular fuel register N3, located outside the swirl register, the NO_x emissions are of the same magnitude as the flames formed from using registers N6 and N5 with a high amount of primary air. A slight increase in NO_x formation with increasing the amount of primary air can be observed also for N3.

In contrast, when co-firing coal with biomass, the NO_x emissions decrease with an increase in the level of primary air. Modeling of the aerodynamics is needed to pinpoint the exact reason from this. However, the biomass contains scarcely any nitrogen, so an increase in local stoichiometry around the biomass particles would not increase significantly the amount of NO_x formed. It is possible that the higher level of primary air facilitates the combustion of the biomass particles, and that the released volatiles from these to some extent shield the coal particles from the secondary air. Although this is pure speculation, it is a possibility that should be explored in future co-firing experiments.

Figure 22 presents the in-flame measurements for two cases with different amounts of primary air (marked with red symbols in Figure 21). The high levels of O_2 and the low levels of CO observed in the case with a high level of primary air suggest that the flame is lifted, and that significant amount of air has been entrained prior to ignition. Lifted flames were observed for most other fuels combusted with a high level of primary air. When a low amount of primary air was used, a hot O_2-lean zone was detected in front of the burner, indicating an attached flame. The formation of such zones is known to be paramount for reducing NO formation from fuel-bound nitrogen.

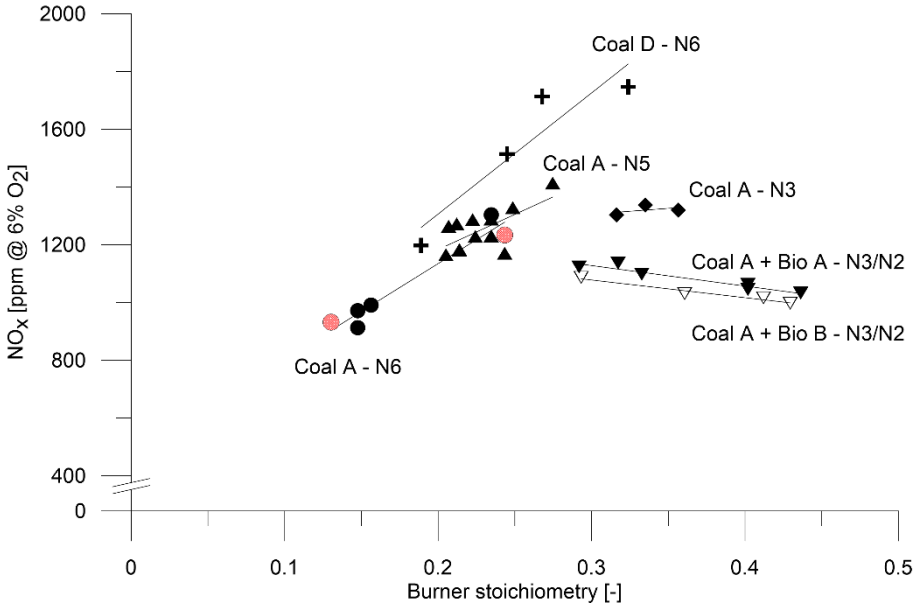

Figure 21. Level of NO_x emissions in relation to burner stoichiometry, burner register, and fuel type. Note the y-axis break. The symbols marked in red represent flames in which in-flame measurements were performed.

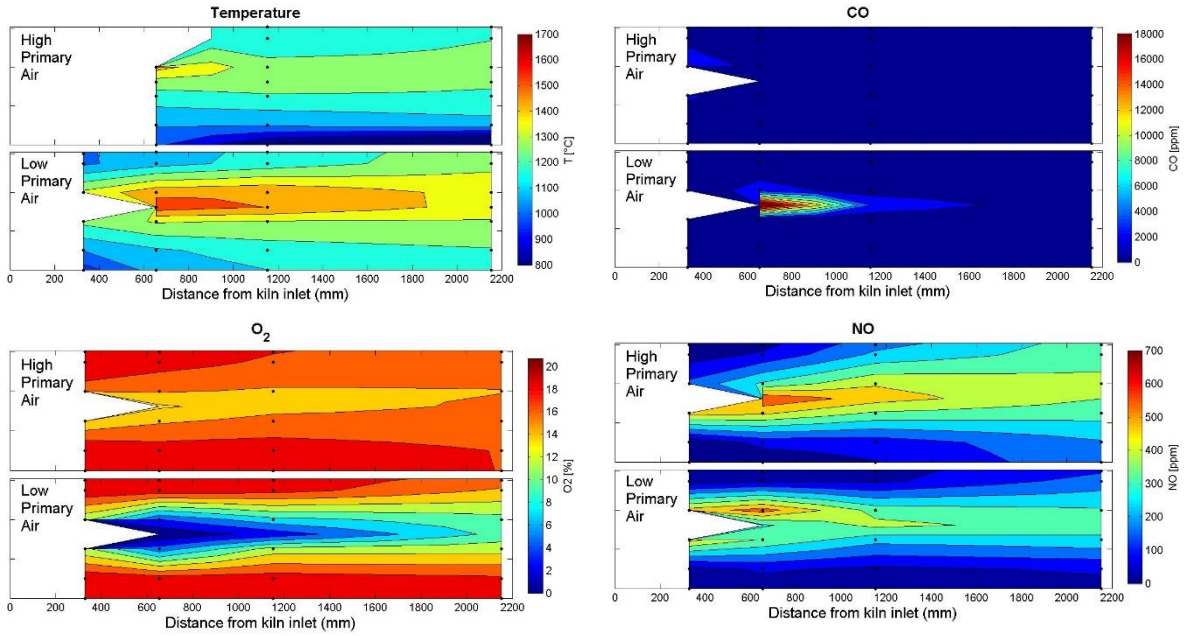

Figure 22. Filled contour maps for temperature, CO, O_2, and NO for two cases: one with a high level of primary air and one with a low level of primary air in the kiln. These flames are marked with red symbols in Figure 21.

7.4 NO_x mitigation measures

For conventional combustion units, for example plants in the heat and power industry, a combination of primary and secondary measures is often used to comply with emission regulations. The LKAB KK4 plant was the first Grate-Kiln plant to implement a secondary measure in the form of a SCR. Bolen [28] writes that this plant marked the start of a new era in pollution control for the production of iron ore. The installed SCR succeeds in reducing NO_x efficiently when running. However, the large volumetric gas flow, the dusty environment and the inherent variations in operating conditions make the SCR costly to run and it is not easily integrated in the process. For practical reasons, the SCR is therefore often bypassed. Primary measures are thus preferred.

Over the years, a significant number of tests has been conducted by LKAB with the aim of reducing NO_x emissions. The original goal was to reduce NO_x in the full-scale kiln with 40% by using primary measures. This section presents the measures that have been applied in both pilot-scale and full-scale and the corresponding NO_x reductions. Suggestions for future NO_x mitigation measures are provided by the end.

Summary of tested primary measures

Table 8 lists the primary measures for NO_x reduction that have been tested by LKAB in the pilot-scale and full-scale kilns (reviewed in **Paper IV**). It is evident from the table that the goal of achieving 40% NO_x reduction has not been accomplished. Since the pilot-scale kiln has been rebuilt several times, it is not possible to relate all measures to one baseline value. It can however be established that the measures that achieve NO_x reduction in pilot-scale only achieve modest NO_x reductions in the full-scale. This is to some extent expected given that the initial NO level is higher in the pilot-scale kiln and that a higher NO partial pressure will facilitate both the homogeneous and heterogeneous reduction of NO. Some measures, e.g., the use of water sprays, aim to reduce thermal NO formation; the fact that the NO_x emissions are not reduced is in line with the low-level importance of thermal NO discussed in the previous section. Primary measures that target the reduction of vol-N conversion, such as burner design

and burner air flow configuration, achieve noteworthy reductions in pilot-scale but fail to reduce NO_x significantly in full-scale.

Table 8. A summary of the primary measures for NO_x reduction that have been tested by LKAB in pilot-scale and full-scale kilns.

Primary measure	**Description**	**NO_x reduction pilot-scale**	**NO_x reduction full-scale**
Low NO_x burners	'Precessing jet' burner	15%	0%
	'Large swirl' burner	10%	5%
Kiln hood modifications	Reduced mixing intensity of secondary air	10%	5%
Decreased secondary air temperature	From 1080°C to 970°C	0%–15%*	Not tested
Heating of primary air	340°C	0%	Not tested
Heating of coal	85°C	0%	Not tested
Reducing excess air	λ: 4.6 → 4.3	Not tested	8.5%**
	λ: 4.0 → 1.1	5%–50%	Not tested
Reducing primary air	λ_{burner}: 0.25 → 0.13	25%***	Not tested
Increasing transport air velocity		0%	0%–10%
Propane co-firing		0%	Not tested
Primary air partly replaced by steam, N_2 or Ar		0%	Not tested
Addition of water sprays around burner		0%	Not tested
Addition of water to the secondary air		0%	Not tested

* Only reduced NO_x in the absence of a cooling system to represent the pellet bed
** Resulted in pellet quality problems
*** Change from lifted flame to attached flame

One of the most efficient ways to reduce NO_x formation in both pilot-scale and full-scale is to reduce the amount of excess air. By only reducing it slightly in full-scale, a reduction of 8.5% is achieved. The strong effect of excess air is supported by modelling. Figure 23 presents simulation results (from **Paper IV**) for reductions in stoichiometry so that the exit O_2 concentration went from 16% to 13% and 10% respectively. The reduction in excess air reduces primarily the amount of NO formed the heterogeneous reactions, although a slight reduction in the homogeneous contribution can also be observed. However, as noted in Table 8, the reduction of excess air also resulted in issues with the pellet quality.

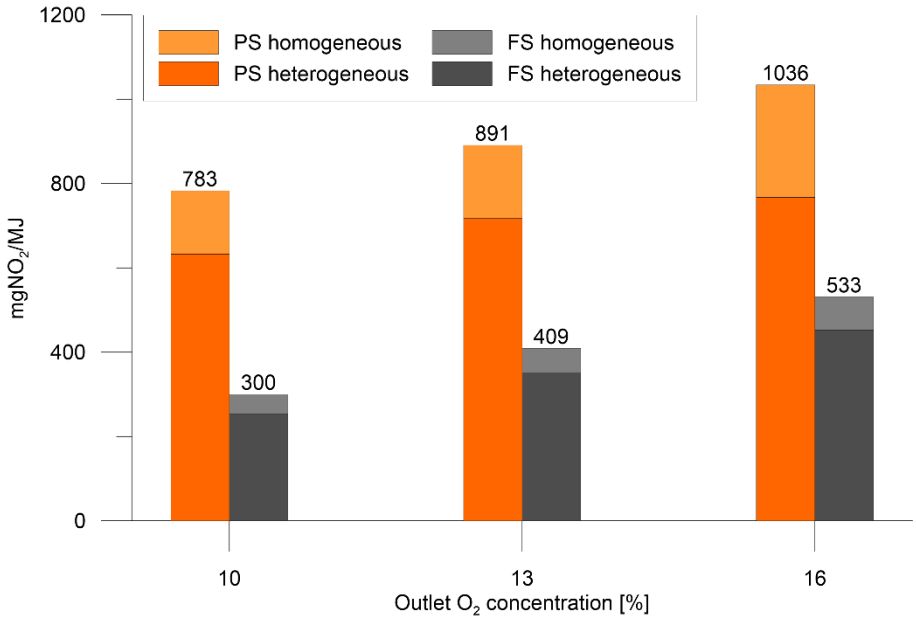

Figure 23. NO formation in pilot-scale and full-scale as a function of excess air. For these simulations, the amount of primary air is high (λ_{burner} = 0.25). PS: pilot-scale kiln; FS: full-scale kiln; homogeneous: net NO formation from homogeneous reactions (including vol-N conversion and thermal NO formation); heterogeneous: net NO formation from the oxidation of char-N and the reduction of NO by char.

Apart from reducing the amount of excess air, increasing the transport air is the only primary measures that has had any significant effect in full-scale. Boateng [78] writes that for confined jet flames, high primary air velocities recirculates combustion products to the burner and thus facilitates an attached flame. This is a likely explanation, although in the pilot-scale flame, high amounts of primary air resulted in lifted flames, which is also in-line with the results from other work on pilot-scale kilns, e.g. the CEMFLAME project [89, 90].

Proposed mitigation measures

Based on the results presented in this chapter, measures for efficient NO_x reduction in iron ore rotary kilns should focus on:

A) Addressing the high char-N conversion to NO; and/or

B) Reducing the amount of nitrogen in the char

Regarding point A), the high conversion of char-N is primarily an effect of the high level of excess air, since it leads to high concentrations of O_2 and also dilutes the formed NO, making NO reduction reactions less-efficient. However, because the reduction of excess air resulted in problems with product quality, it is not a viable option in the absence of actions to adapt the heat treatment process. An alternative way to reduce the high char-N conversion is to apply burners that do not produce jet flames (i.e., not Type-0 flames), such that more of the char is combusted and gasified in an internal recirculation zone in front of the burner. Results from a flat-burner flame was used as input to the model in **Paper IV** and showed that the gasification of char and char-N results in considerably lower NO_x emissions. Type 1-3 flames are significantly shorter than Type-0 (jet) flames, and an evaluation of the impact on pellet quality would need to be made. It is also not clear whether such flames can be maintained given the large flow of secondary air.

Regarding point B), the model suggests that if the nitrogen could be released with the volatiles rather than being retained in the char, NO formation would be reduced drastically. In theory, this could be achieved by increasing the pyrolysis temperature. This concept has been

successfully demonstrated by Bool and Bradley [102], who injected small amounts of O_2 into swirled flames. The injection of O_2 increased the local temperature and drove off the nitrogen. However, the level of O_2 must be low, to ensure that the local conditions remain sub-stoichiometric. This application could be of interest to test in iron ore rotary kilns, although a jet flame has a less-pronounced reducing zone than a swirling flame, which raises a challenging issue. Other measures to increase the pyrolysis temperature include pre-heating the primary air and fuel, although as shown in Table 8, this approach has not proved successful in pilot-scale.

A more drastic and straight-forward alternative would be to eliminate the fuel-N altogether. Since the co-firing cases with biomass reduced NO_x emissions almost linearly with nitrogen content in the pilot-scale kiln, increasing the biomass share should continue to decrease the NO_x emissions. LKAB has plans to trial 100% biofuel combustion to reduce their CO_2 emissions [103], which can also reduce their NO_x emissions as long as the nitrogen content is low. Figure 24 shows simulations with 30% and 100% biomass replacement, with the biomass containing 0.1% nitrogen. According to these simulations, NO_x can be reduced by 90% by the usage of biomass. To successfully implement this, it is important to evaluate how it would impact the pellet quality in terms of changes to the heat transfer between flame, walls and pellets in the kiln.

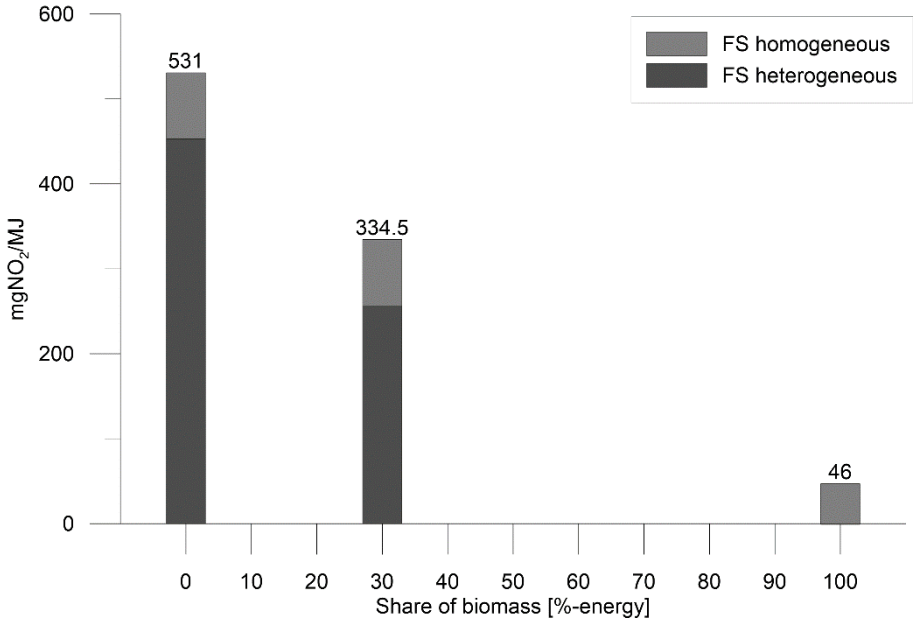

Figure 24. Modelled NO_x formation as a function of biomass replacement of coal in the full-scale kiln. FS: full-scale kiln; homogeneous: net NO formation from homogeneous reactions (including vol-N conversion and thermal NO formation); heterogeneous: net NO formation from the oxidation of char-N and the reduction of NO by char.

7.5 Comparison to a conventional state-of-the-art flame

Of the flames investigated in this work, the L1500 swirl flame **(Paper V**) is the one that can be considered most state-of-the-art in terms of NO_x control for flames, since it is not a Type-0 flame and also applies OFA staging. Figure 25 presents a compilation of the NO_x emissions from the flames investigated in this work normalized to the fuel-N as a function of the convective mixing time (based on the 'burner' values listed in Table 3). The L1500 swirl flame has clearly a lower level of NO_x emission than any of the Type-0 flames. The Type-0 flames correlate well with the convective mixing time, although additional flames would have to be added to confirm that the convective mixing time is a good indicator for NO_x formation.

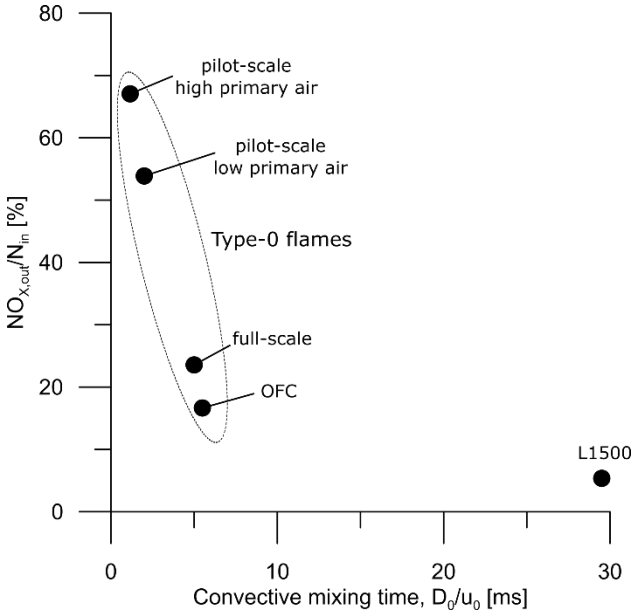

Figure 25. Ratio of outgoing NO_x to ingoing fuel-nitrogen as a function of the convective mixing time based on the combustion facilities used in this work.

Figure 26 compares the in-flame measurements of temperature, CO, and NO for the pilot-scale kiln flame, the OFC flame and the L1500 swirl flame. The flame in the pilot-scale kiln is the same as shown in Figure 22 when a low amount of primary air was used. The two axes are normalized to the burner diameter of the respective burner. Starting from the right-hand side, the L1500 swirl flame has a hot reducing region in front of the burner, indicating a strong recirculation zone. This is an effect of the sub-stoichiometric conditions of the burner and the swirled air registers. Additionally, the low velocity of the fuel stream (facilitated by the use of OFA staging) likely results in a significant particle residence time in this zone. NO is formed at high concentrations in the beginning of the furnace, to the right of the burner, although the concentration of NO rapidly decreases. To the left of the burner, the NO concentration is significantly lower. This agrees with the higher CO concentration on the left-hand side, signifying a more reducing environment.

The temperatures were significantly lower in the OFC flame and no reducing zone was observed. Compared to the L1500 case, measurements were not performed in the early part of the flame, and it is possible that a reducing zone exists there. However, since it is a jet flame it is unlikely that it is as reducing as the L1500 flame. The NO concentration increases along the length of the OFC, indicating that the particles are burning far from the burner and that NO is being formed continuously.

Regarding the pilot-scale kiln flame, the temperatures near the burner are similar to those observed in the L1500 swirl flame. However, the CO concentrations are significantly lower (peak concentration of 2.2% compared to 9.3%), and the residence time in this zone is significantly shorter in the pilot-scale kiln due to the nature of jet flames. The NO concentration in the stack is 367 ppm, although the average spatial concentration of NO in the last measurement port is clearly below this value, confirming that NO formation continues in the later part of the kiln (i.e., there is significant formation of NO from char combustion).

Achieving the same reducing conditions in a rotary kiln flame as observed in the L1500 flame is not realistic due to the requirement of excess air and the fact that the kiln rotation prevents external staging. This work has shown that optimizing the burner configuration can enhance the formation of a sub-stoichiometric zone in front of the burner where vol-N conversion is suppressed, and where char is to some extent gasified. The inherent high particle velocity in jet

flames will however prevent significant residence time in such zones. These results emphasize the need to either eliminate the fuel-bound nitrogen or turn to secondary measures.

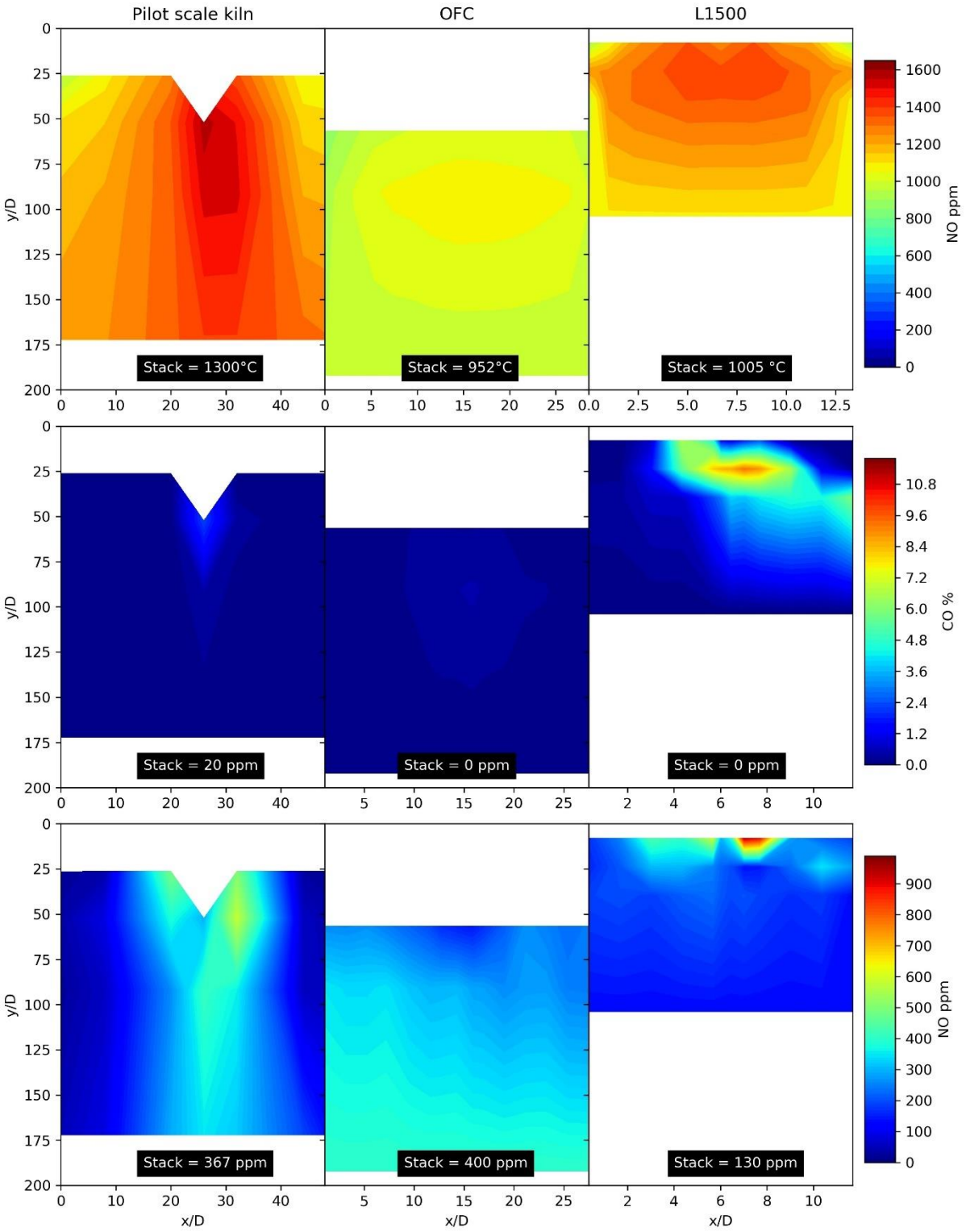

Figure 26. In-flame measurements of temperature, CO, and NO in the pilot-scale kiln, the OFC, and the L1500. The axes are normalized to the burner diameter of the specific combustion unit.

8 Conclusion

This thesis investigates the formation of NO_x in iron ore rotary kilns. The reaction routes for NO formation in the Type-0 flame used have been mapped and evaluated through detailed reaction modeling and a series of measurement campaigns in different units and at different scales.

The mapping of the reaction routes reveal that the formation of NO_x is mainly from the fuel-bound nitrogen, and that the design of the solid-fuel firing system manages to suppress thermal formation of NO. This finding, which is discordant with the findings of previous studies on rotary kilns, will have an important impact on efforts to design efficient primary measures. This thesis concludes that the high concentrations of oxygen required to sustain the iron ore oxidation process increase significantly the rate of mainly char-N to NO conversion.

The mapping of the reaction routes and the evaluation of the constant velocity scaling principle for the Type-0 flame also explain the modest effects seen previously for low-NO_x techniques tested in the full-scale rotary kiln. This work proposes that future efforts should focus on reducing the amount of char-bound nitrogen through: A) shifting to a low-N fuel; or B) increasing the share of nitrogen released with the volatiles.

9 Outlook

Implementation of (low-nitrogen) biomass combustion in full-scale shows promising effects on NO_x reduction by the work performed in this thesis and is thus a recommended for future work. Efforts are being made by LKAB to reduce their CO_2 emissions, and full-scale biomass combustion could become reality in the coming years.

Suggestions for additional future work includes evaluating the effect of char characteristics on NO_x and developing the modeling approach. Since the char-NO interaction is controlling the NO formation in rotary kiln flames, investigating how to enhance the NO reduction by char would be interesting. For example, the influence of ash minerals or fuel properties that affect the char surface area could be investigated. Furthermore, adapting the heterogeneous kinetics to the fuel (e.g., type and particle size) and to the combustion conditions relevant for rotary kilns is recommended for a more accurate description of the NO-char interaction. A particle model could be developed to complement the model.

Finally, an aspect that has not been covered in this work is the potential interaction between the pellet bed and the NO_x gases in full-scale. Both the iron oxide and the binding ingredients in the pellets could potentially reduce NO_x under the right circumstances. Establishing whether such effects should be considered, or taken advantage of, would be useful.

References

[1] J. Lelieveld, K. Klingmuller, A. Pozzer, U. Poschl, M. Fnais, A. Daiber, and T. Munzel, "Cardiovascular disease burden from ambient air pollution in Europe reassessed using novel hazard ratio functions," *European Heart Journal,* vol. 40, no. 20, pp. 1590-1596, May 21 2019.

[2] "Ambient air pollution: A global assessment of exposure and burden of disease," World Health Organization9241511354, 2016.

[3] A. J. Cohen, M. Brauer, R. Burnett, H. R. Anderson, J. Frostad, K. Estep, K. Balakrishnan, B. Brunekreef, L. Dandona, R. Dandona, V. Feigin, G. Freedman, B. Hubbell, A. Jobling, H. Kan, L. Knibbs, Y. Liu, R. Martin, L. Morawska, C. A. Pope, H. Shin, K. Straif, G. Shaddick, M. Thomas, R. van Dingenen, A. van Donkelaar, T. Vos, C. J. L. Murray, and M. H. Forouzanfar, "Estimates and 25-year trends of the global burden of disease attributable to ambient air pollution: an analysis of data from the Global Burden of Diseases Study 2015," *The Lancet,* vol. 389, no. 10082, pp. 1907-1918, 2017/05/13/ 2017.

[4] M. Brauer, G. Freedman, J. Frostad, A. van Donkelaar, R. V. Martin, F. Dentener, R. v. Dingenen, K. Estep, H. Amini, J. S. Apte, K. Balakrishnan, L. Barregard, D. Broday, V. Feigin, S. Ghosh, P. K. Hopke, L. D. Knibbs, Y. Kokubo, Y. Liu, S. Ma, L. Morawska, J. L. T. Sangrador, G. Shaddick, H. R. Anderson, T. Vos, M. H. Forouzanfar, R. T. Burnett, and A. Cohen, "Ambient Air Pollution Exposure Estimation for the Global Burden of Disease 2013," *Environmental Science & Technology,* vol. 50, no. 1, pp. 79-88, 2016/01/05 2016.

[5] H. Olstrup, B. Forsberg, H. Orru, M. Spanne, H. Nguyen, P. Molnar, and C. Johansson, "Trends in air pollutants and health impacts in three Swedish cities over the past three decades," (in English), *Atmospheric Chemistry and Physics,* vol. 18, no. 21, pp. 15705-15723, Nov 1 2018.

[6] A. W. Correia, C. Arden Pope, D. W. Dockery, Y. Wang, M. Ezzati, and F. Dominici, "Effect of air pollution control on life expectancy in the United States: An analysis of 545 U.S. Counties for the period from 2000 to 2007," *Epidemiology,* Article vol. 24, no. 1, pp. 23-31, 2013.

[7] A. S. V. Shah, J. P. Langrish, H. Nair, D. A. McAllister, A. L. Hunter, K. Donaldson, D. E. Newby, and N. L. Mills, "Global association of air pollution and heart failure: a systematic review and meta-analysis," *The Lancet,* vol. 382, no. 9897, pp. 1039-1048, 2013/09/21/ 2013.

[8] R. Bobbink, M. Hornung, and J. G. M. Roelofs, "The effects of air-borne nitrogen pollutants on species diversity in natural and semi-natural European vegetation," *Journal of Ecology,* Review vol. 86, no. 5, pp. 717-738, 1998.

[9] E. A. Ainsworth, C. R. Yendrek, S. Sitch, W. J. Collins, and L. D. Emberson, "The effects of tropospheric ozone on net primary productivity and implications for climate change," *Annual Review of Plant Biology,* vol. 63, pp. 637-61, 2012.

[10] J. Rose, *Acid rain: current situation and remedies*. Yverdon: Gordon and Breach, 1994.

[11] C. Vovelle, *Pollutants from combustion: formation and impact on atmospheric chemistry*. Springer Science & Business Media, 2013.

[12] M. Z. Jacobson, *Atmospheric pollution: history, science, and regulation*. Cambridge University Press, 2002.

[13] M. L. Bell, D. L. Davis, and T. Fletcher, "A retrospective assessment of mortality from the London smog episode of 1952: the role of influenza and pollution," *Environmental health perspectives*, vol. 112, no. 1, p. 6, 2004.

[14] S. Sillman, "Tropospheric ozone and photochemical smog," *Environmental geochemistry*, vol. 9, pp. 407-31, 2003.

[15] S. Manahan, *Environmental chemistry*. CRC press, 2017.

[16] U. Kulshrestha, "Acid rain," vol. 1, ed: Taylor & Francis, New York, 2013, pp. 8-22.

[17] T. Rafstedt, "Effekter av kalkning på myrvegetation," in "Havs-och vattenmyndighetens rapport 2016:19," Havs-och vattenmyndigheten2016, Available: https://www.havochvatten.se/hav/uppdrag--kontakt/publikationer/publikationer/2016-09-30-effekter-av-kalkning-pa-myrvegetation.html.

[18] M. Muntean, D. Guizzardi, E. Schaaf, M. Crippa, E. Solazzo, J. Olivier, and E. Vignati, "Fossil CO2 Emissions of All World Countries-2018 Report," 2018.

[19] M. Crippa, D. Guizzardi, M. Muntean, E. Schaaf, F. Dentener, J. A. v. Aardenne, S. Monni, U. Doering, J. G. Olivier, and V. Pagliari, "Gridded emissions of air pollutants for the period 1970–2012 within EDGAR v4. 3.2," *Earth System Science Data*, vol. 10, no. 4, pp. 1987-2013, 2018.

[20] Naturvårdsverket. Utsläpp i siffror [Online].

[21] "World Steel in Figures 2019," World Steel Association 2019, Available: https://www.worldsteel.org/media-centre/press-releases/2019/world-steel-in-figures-2019.html.

[22] S. Pauliuk, T. Wang, and D. B. Muller, "Steel all over the world: Estimating in-use stocks of iron for 200 countries," *Resources Conservation and Recycling*, vol. 71, pp. 22-30, Feb 2013.

[23] D. B. Müller, T. Wang, and B. Duval, "Patterns of Iron Use in Societal Evolution," *Environmental Science & Technology*, vol. 45, no. 1, pp. 182-188, 2011/01/01 2011.

[24] P. Mbele, "Pelletizing of Sishen concentrate," *Journal of the Southern African Institute of Mining and Metallurgy*, vol. 112, no. 3, pp. 221-228, 2012.

[25] D. Zhu, J. Pan, L. Lu, and R. J. Holmes, "Iron ore pelletization," in *Iron Ore*: Elsevier, 2015, pp. 435-473.

[26] J. Mourão, M. Huerta, U. de Medeiros, I. Cameron, K. O'Leary, and C. Howey, "Guidelines for selecting pellet plant technology," in *Proceedings of the 6th International Congress on the Science and Technology of Ironmaking–ICSTI*, 2012.

[27] N.-O. Lindfors and P. Kostamo, *BAT examples from the Nordic iron and steel industry*. Nordic Council of Ministers, 2006.

[28] J. Bolen, "Modern air pollution control for iron ore induration," *Minerals & Metallurgical Processing*, vol. 31, no. 2, pp. 103-114, 2014.

[29] D. W. Pershing and J. O. L. Wendt, "Pulverized coal combustion: The influence of flame temperature and coal composition on thermal and fuel NOx," in *Symposium (International) on Combustion*, 1977, vol. 16, no. 1, pp. 389-399: Elsevier.

[30] Y. Zeldovich, D. Frank-Kamenetskii, and P. Sadovnikov, *Oxidation of nitrogen in combustion*. Publishing House of the Acad of Sciences of USSR, 1947.

[31] R. P. van der Lans, P. Glarborg, and K. Dam-Johansen, "Influence of process parameters on nitrogen oxide formation in pulverized coal burners," *Progress in Energy and Combustion Science*, vol. 23, no. 4, pp. 349-377, // 1997.

[32] P. Glarborg, A. D. Jensen, and J. E. Johnsson, "Fuel nitrogen conversion in solid fuel fired systems," (in English), *Progress in Energy and Combustion Science*, vol. 29, no. 2, pp. 89-113, 2003.

[33] H. Zhang and T. H. Fletcher, "Nitrogen transformations during secondary coal pyrolysis," *Energy & fuels*, vol. 15, no. 6, pp. 1512-1522, 2001.

[34] D. W. Blair, J. O. L. Wendt, and W. Bartok, "Evolution of nitrogen and other species during controlled pyrolysis of coal," in *Symposium (International) on Combustion*, 1977, vol. 16, no. 1, pp. 475-489: Elsevier.

[35] J. H. Pohl and A. F. Sarofim, "Devolatilization and oxidation of coal nitrogen," in *Symposium (International) on Combustion*, 1977, vol. 16, no. 1, pp. 491-501: Elsevier.

[36] P. R. Solomon and M. B. Colket, "Evolution of fuel nitrogen in coal devolatilization," *Fuel*, vol. 57, no. 12, pp. 749-755, 1978.

[37] S. Kambara, T. Takarada, Y. Yamamoto, and K. Kato, "Relation between functional forms of coal nitrogen and formation of nitrogen oxide (NOx) precursors during rapid pyrolysis," *Energy & Fuels*, vol. 7, no. 6, pp. 1013-1020, 1993.

[38] P. R. Solomon, D. G. Hamblen, M. A. Serio, Z.-Z. Yu, and S. Charpenay, "A characterization method and model for predicting coal conversion behaviour," *Fuel*, vol. 72, no. 4, pp. 469-488, 1993.

[39] S. Niksa, "FLASHCHAIN theory for rapid coal devolatilization kinetics. 3. Modeling the behavior of various coals," *Energy & Fuels*, vol. 5, no. 5, pp. 673-683, 1991.

[40] T. H. Fletcher, A. R. Kerstein, R. J. Pugmire, M. Solum, and D. M. Grant, "A chemical percolation model for devolatilization: summary," *Brigham Young University*, 1992.

[41] J. O. L. Wendt and C. V. Sternling, "Effect of ammonia in gaseous fuels on nitrogen oxide emissions," *Journal of the Air Pollution Control Association,* vol. 24, no. 11, pp. 1055-1058, 1974.

[42] J. A. Miller and C. T. Bowman, "Mechanism and Modeling of Nitrogen Chemistry in Combustion," (in English), *Progress in Energy and Combustion Science,* vol. 15, no. 4, pp. 287-338, 1989/01/01 1989.

[43] G. P. Smith, D. M. Golden, M. Frenklach, N. W. Moriarty, B. Eiteneer, M. Goldenberg, C. Bowman, R. Hanson, S. Song, and W. Gardiner Jr. GRI-Mech 3.0, 2000 [Online].

[44] J. C. Chen and S. Niksa, "Suppressed nitrogen evolution from coal-derived soot and low-volatility coal chars," *Symposium (International) on Combustion,* vol. 24, no. 1, pp. 1269-1276, 1992/01/01 1992.

[45] G. J. Haussmann and C. H. Kruger, "Evolution and reaction of coal fuel nitrogen during rapid oxidative pyrolysis and combustion," *Symposium (International) on Combustion,* vol. 23, no. 1, pp. 1265-1271, 1991/01/01 1991.

[46] J. C. Chen, C. Castagnoli, and S. Niksa, "Coal devolatilization during rapid transient heating. 2. Secondary pyrolysis," *Energy & Fuels,* vol. 6, no. 3, pp. 264-271, 1992.

[47] M. T. Cheng, M. J. Kirsch, and T. W. Lester, "Reaction of nitric oxide with bound carbon at flame temperatures," *Combustion and Flame,* vol. 77, no. 2, pp. 213-217, 1989/08/01 1989.

[48] M. Østberg, P. Glarborg, A. Jensen, J. E. Johnsson, L. S. Pedersen, and K. Dam-Johansen, "A model of the coal reburning process," *Symposium (International) on Combustion,* vol. 27, no. 2, pp. 3027-3035, 1998/01/01 1998.

[49] D. Phong-Anant, L. Wibberley, and T. Wall, "Nitrogen oxide formation from Australian coals," *Combustion and flame,* vol. 62, no. 1, pp. 21-30, 1985.

[50] Y. H. Song, J. H. Pohl, J. M. Beer, and A. F. Sarofim, "Nitric-Oxide Formation during Pulverized Coal Combustion," (in English), *Combustion Science and Technology,* vol. 28, no. 1-2, pp. 31-39, 1982.

[51] J. P. Spinti and D. W. Pershing, "The fate of char-N at pulverized coal conditions," *Combustion and Flame,* vol. 135, no. 3, pp. 299-313, 2003.

[52] D. W. Pershing and J. O. L. Wendt, "Relative contributions of volatile nitrogen and char nitrogen to NOx emissions from pulverized coal flames," *Industrial & Engineering Chemistry Process Design and Development,* vol. 18, no. 1, pp. 60-67, 1979.

[53] A. Molina, E. G. Eddings, D. W. Pershing, and A. F. Sarofim, "Nitric oxide destruction during coal and char oxidation under pulverized-coal combustion conditions," *Combustion and Flame,* vol. 136, no. 3, pp. 303-312, 2// 2004.

[54] P. F. Nelson, P. C. Nancarrow, J. Bus, and A. Prokopiuk, "Fractional conversion of char N to NO in an entrained flow reactor," *Proceedings of the Combustion Institute,* vol. 29, no. 2, pp. 2267-2274, 2002.

[55] L. S. Jensen, H. E. Jannerup, P. Glarborg, A. Jensen, and K. Dam-Johansen, "Experimental investigation of NO from pulverized char combustion," *Proceedings of the Combustion Institute,* vol. 28, no. 2, pp. 2271-2278, 2000.

[56] K. Zhao, P. Glarborg, and A. D. Jensen, "NO reduction over biomass and coal char during simultaneous combustion," *Energy & Fuels,* vol. 27, no. 12, pp. 7817-7826, 2013.

[57] A. Molina, J. J. Murphy, F. Winter, B. S. Haynes, L. G. Blevins, and C. R. Shaddix, "Pathways for conversion of char nitrogen to nitric oxide during pulverized coal combustion," *Combustion and Flame,* vol. 156, no. 3, pp. 574-587, 2009.

[58] S. P. Visona and B. R. Stanmore, "Modeling NOx release from a single coal particle II. Formation of NO from char-nitrogen," *Combustion and Flame,* vol. 106, no. 3, pp. 207-218, 1996.

[59] T. Shimizu, Y. Sazawa, T. Adschiri, and T. Furusawa, "Conversion of Char-Bound Nitrogen to Nitric-Oxide during Combustion," (in English), *Fuel,* vol. 71, no. 4, pp. 361-365, Apr 1992.

[60] W. Wang, S. D. Brown, C. J. Hindmarsh, and K. M. Thomas, "NOx release and reactivity of chars from a wide range of coals during combustion," *Fuel,* vol. 73, no. 9, pp. 1381-1388, 1994.

[61] I. Glassman and R. A. Yetter, "Chapter 9 - Combustion of Nonvolatile Fuels," in *Combustion (Fourth Edition)*Burlington: Academic Press, 2008, pp. 495-550.

[62] R. H. Hurt and J. M. Calo, "Semi-global intrinsic kinetics for char combustion modeling," *Combustion and Flame,* vol. 125, no. 3, pp. 1138-1149, 2001/05/01/ 2001.

[63] R. Barranco, A. Rojas, J. Barraza, and E. Lester, "A new char combustion kinetic model 1. Formulation," *Fuel,* vol. 88, no. 12, pp. 2335-2339, 2009/12/01/ 2009.

[64] W. Chen, L. Smoot, S. Hill, and T. Fletcher, "Global rate expression for nitric oxide reburning. Part 2," *Energy & fuels,* vol. 10, no. 5, pp. 1046-1052, 1996.

[65] B. Coda, F. Kluger, D. Förtsch, H. Spliethoff, K. Hein, and L. Tognotti, "Coal-nitrogen release and NOx evolution in air-staged combustion," *Energy & fuels,* vol. 12, no. 6, pp. 1322-1327, 1998.

[66] I. Aarna and E. M. Suuberg, "A review of the kinetics of the nitric oxide-carbon reaction," *Fuel,* vol. 76, no. 6, pp. 475-491, 1997.

[67] Y. H. Song, J. M. Beér, and A. F. Sarofim, "Reduction of Nitric Oxide by Coal Char at Temperatures of 1250–1750 K," *Combustion Science and Technology,* vol. 25, no. 5-6, pp. 237-240, 2008.

[68] L. Chan, A. Sarofim, and J. Beer, "Kinetics of the NO□ carbon reaction at fluidized bed combustor conditions," *Combustion and Flame,* vol. 52, pp. 37-45, 1983.

[69] A.-K. Hjalmarsson, *NOx control technologies for coal combustion*. IEA Coal Research, 1990.

[70] M. Sami, K. Annamalai, and M. Wooldridge, "Co-firing of coal and biomass fuel blends," *Progress in Energy and Combustion Science*, vol. 27, no. 2, pp. 171-214, 2001/01/01/ 2001.

[71] G. Salvi and R. Payne, "Investigation Into the Scaling of Combustion Systems: A Report on the 018 and 019 Trials Carried Out Piecemeal in the Period from December 1978 to June 1980," International Flame Research Foundation, IJmuidenF 31/a/52, 1981.

[72] J. Smart and D. Morgan, "Exploring the effects of employing different scaling criteria on swirl stabilised pulverised coal burner performance," *Combustion science and technology*, vol. 100, no. 1-6, pp. 331-343, 1994.

[73] T.-C. A. Hsieh, W. J. Dahm, and J. F. Driscoll, "Scaling laws for NOx emission performance of burners and furnaces from 30 kW to 12 MW," *Combustion and Flame*, vol. 114, no. 1-2, pp. 54-80, 1998.

[74] R. Weber, "Scaling characteristics of aerodynamics, heat transfer, and pollutant emissions in industrial flames," in *Symposium (International) on Combustion*, 1996, vol. 26, no. 2, pp. 3343-3354: Elsevier.

[75] D. D. Toporov, "Chapter 6 - Coal Combustion in CO2/O2 Atmosphere," in *Combustion of Pulverised Coal in a Mixture of Oxygen and Recycled Flue Gas*, D. D. Toporov, Ed. Boston: Elsevier, 2014, pp. 111-139.

[76] R. Weber and M. Mancini, "On scaling and mathematical modelling of large scale industrial flames," *Journal of the Energy Institute*, 2019/04/10/ 2019.

[77] C. Baukal and P. Eleazer, "Quantifying NOx for industrial combustion processes," *Journal of the Air & Waste Management Association*, vol. 48, no. 1, pp. 52-58, 1998.

[78] A. A. Boateng, *Rotary kilns: transport phenomena and transport processes*. Butterworth-Heinemann, 2008.

[79] F. Akgun, "Investigaton of energy saving and NOx reduction possibilities in a rotary cement kiln," *International journal of energy research*, vol. 27, no. 4, pp. 455-465, 2003.

[80] G. L. Young, "NOx formation in rotary kilns producing cement clinker applicable NOx control techniques and cost effectiveness of these control techniques," in *IEEE-IAS/PCS 2002 Cement Industry Technical Conference. Conference Record (Cat. No. 02CH37282)*, 2002, pp. 239-254: IEEE.

[81] C. Y. C. Jonsson, J. Stjernberg, H. Wiinikka, B. Lindblom, D. Bostrom, and M. Ohman, "Deposit Formation in a Grate-Kiln Plant for Iron-Ore Pellet Production. Part 1: Characterization of Process Gas Particles," (in English), *Energy & Fuels*, vol. 27, no. 10, pp. 6159-6170, Oct 2013.

[82] LKAB. (2017). *Pelletizing*. Available: https://www.lkab.com/en/about-lkab/from-mine-to-port/processing/pelletizing/

[83] A. T. McQueen, S. J. Bortz, M. S. Hatch, and R. L. Leonard, "Cement Kiln NOx Control," *IEEE Transactions on Industry Applications*, vol. 31, no. 1, pp. 36-44, 1995.

[84] X.-Z. Feng, O. Lugovoy, and H. Qin, "Co-controlling CO2 and NOx emission in China's cement industry: An optimal development pathway study," *Advances in Climate Change Research,* vol. 9, no. 1, pp. 34-42, 2018.

[85] J.-m. Li and G.-d. Li, "Present situation and countermeasures of nitrogen oxides emissions in Chinese cement industry," *Appl Chem Ind,* vol. 42, no. 9, pp. 1687-1689, 2013.

[86] S. Frauke, K. Ioanna, S. B. Maria, R. Serge, and D. S. Luis, "Best Available Techniques (BAT) Reference Document for the Production of Cement, Lime and Magnesium Oxide: Industrial Emissions Directive 2010/75/EU:(Integrated Pollution Prevention and Control)," 2013.

[87] ADEME, "The French Cement Industry Guide to NOx Emissions Reduction Measures," 2002, Available: https://www.ademe.fr/french-cement-industry-guide-to-nox-emissions-reduction-measures.

[88] M. H. Vaccaro, "Low NOx rotary kiln burner technology: design principles & case study," in *Cement Industry Technical Confernece, 2002. IEEE-IAS/PCA 44th*, 2002, pp. 265-270: IEEE.

[89] J. Hass, A. Agostini, C. Martens, E. Carrea, and W. van de Kamp, "The combustion of pulverized coal and alternative fuels in cement kilns. Results on the CEMFLAME-3 experiments," *International Flame Research Foundation (IFRF), IFRF doc no F97/y,* vol. 4, 1999.

[90] W. van de Kamp and J. Daimon, "Further studies on the effect of burner design variables and fuel properties on the characteristics of cement kiln flames—report on the CEMFLAME-2 experiments," *International Flame Research Foundation (IFRF),* 1996.

[91] R. Battye, S. J. Walsh, J. Lee-Greco, and D. Sanders, *NOx Control Technologies for the Cement Industry*. US Environmental Protection Agency, Office of Air Quality Planning and Standards, Air Quality Strategies and Standards Division, 2000.

[92] F. Schorcht, I. Kourti, B. Scalet, S. Roudier, and L. Sancho, "Best Available Techniques (BAT), Reference Document for the Production of Cement, Lime and Magnesium Oxide: Industrial Emissions Directive 2010/75/EU:(Integrated Pollution Prevention and Control)," *JRC Reference Reports; Publications Office of the European Union,* 2013.

[93] R. Remus, M. Aguado Monsonet, S. Roudier, and L. Delgado Sancho, "JRC reference report," *Best Available Techniques (BAT) Reference Document for Iron and Steel Production,* 2013.

[94] R. A. Davis, "Nitric oxide formation in an iron oxide pellet rotary kiln furnace," *Journal of the Air & Waste Management Association,* vol. 48, no. 1, pp. 44-51, 1998.

[95] R. K. Zahl, L. A. Haas, and J. Engesser, "Formation of NOx in iron oxide pelletizing furnaces," University of Minnesota1995.

[96] A. Gunnarsson, "Experimental and numerical studies of thermal radiation in gas, coal and co-fired pilot test facilities," Licentiate thesis, Energy and Environment, Chalmers University of Technology, 2017.

[97] T. Mendiara and P. Glarborg, "Ammonia chemistry in oxy-fuel combustion of methane," *Combustion and Flame,* vol. 156, no. 10, pp. 1937-1949, 10// 2009.

[98] L. S. Jensen, "NOx from cement production-Reduction by Primary Measures," Doctoral thesis, Department of Chemical and Biochemical Engineering, Technical University of Denmark, 1999.

[99] H. Thunman, F. Niklasson, F. Johnsson, and B. Leckner, "Composition of volatile gases and thermochemical properties of wood for modeling of fixed or fluidized beds," *Energy & Fuels,* vol. 15, no. 6, pp. 1488-1497, 2001.

[100] S. L. Chen, M. P. Heap, D. W. Pershing, and G. B. Martin, "Influence of coal composition on the fate of volatileand char nitrogen during combustion," *Symposium (International) on Combustion,* vol. 19, no. 1, pp. 1271-1280, 1982.

[101] *Directive (EU) 2015/2193 of the European Parliament and of the Council of 25 November 2015 on the limitation of emissions of certain pollutants into the air from medium combustion plants (Text with EEA relevance)*, 2015.

[102] L. Bool and J. Bradley, "NOx reduction from a 44 MW wall-fired boiler utilizing oxygen enhanced combustion," in *MEGA Symposium, Washington, DC*, 2003: Citeseer.

[103] LKAB, "HYBRIT: Construction begins – LKAB takes the leap towards fossil-free production of iron ore pellets", Press Release, 2019

APPENDIX A

Conversion of units of NO_x

The two most common ways of reporting NO_x emission are 1) $mgNO_2/MJ$ and 2) ppm (or mg/m^3_n) corrected to an oxygen concentration. When converting one measurement unit to the other, the key is to establish the molar flow of the flue gases.

If NO_x emissions are given in $mgNO_2/MJ$, it is easy to simply multiply by the heat input (fuel input in this work) in MW to get the mass flow of NO_2. Dividing by the molar mass of NO_2 (46 g/mol) yields the molar flow of NO_x (the assumption is that all NO_x eventually converts to NO_2). To get the NO_x concentration one must divide this molar flow by the total molar flow of flue gases. This is not an issue if the flue gas flow is known, but otherwise it must be calculated as:

$$\begin{aligned} n_{tot} &= n_{CO2,out} + n_{H2O,out} + n_{N2,out} + n_{O2,out} \\ &= n_{C,in} + 0.5n_{H,in} + 0.79\lambda N_{0,stoich} + 0.21(\lambda - 1)N_{0,stoich} \end{aligned}$$

where n_{tot} is the flue gas molar flow, $n_{i,out}$ is the molar flow of specie *i* in the flue gases, $n_{i,in}$ is the molar flow of specie *i* by the inlet, $N_{0,stoich}$ is the stoichiometric air demand for the fuel and λ is the stoichiometric ratio. $N_{0,stoich}$ is calculated as:

$$N_{0,stoich} = n_{C,in} + 0.25n_{H,in} - 0.5n_{O,in}$$

Using the values for $n_{i,in}$ from the ultimate analysis of the fuel and using the value of λ (can be calculated with knowledge of the outlet molar fraction of O_2 and $N_{0,stoich}$), the molar flue gas flow can be calculated, and thus also the NO_x molar fraction. When the molar fractions of NO_x and O_2 are known, it is simple to just use Eq.6 to get the ppm value corrected to an oxygen concentration

APPENDIX B

Difference between modelling in Paper II and III

Both Paper II and Paper III conclude that NO formation from the heterogeneous reactions dominate due to the high air-to-fuel ratio in the Grate-Kiln process. However, in Paper II a good fit between modelled and measured NO_x emission is achieved when the nitrogen partitioning is 50/50 between volatiles and char, while in Paper III a good fit is achieved with the nitrogen partitioning being 25/75. This is due to differences in the mixing profiles used for the secondary air.

The mixing profiles of the secondary air used in in Paper II and Paper III are presented in Figure 1 and the resulting O_2 profiles are presented in Figure 2. The mixing is similar in both papers, but in Paper II it is faster in the region stretching from 1000 mm to the end of the kiln, which results in a higher O_2 concentration and thus more NO is formed during the char combustion. The reason for the discrepancy in the mixing profiles is that a smooth profile was desired in Paper III (for smoother scale-up to the full-scale kiln), while the profile in Paper II consisted of only 6 points with linear interpolation between. Fitting a second-order polynomial to the Paper II profile resulted in a faster-than-desired mixing profile during the first 1000 mm (the modelled O_2 and CO profiles did not match the measured values). The polynomial became $0.9863x^2 + 0.2244x-0.0103$, which was reduced to $0.95x^2 + 0.17x$ to fit the O_2 and CO measurements. The mixing profile in Paper III became thus:

$$injected\ air = 740\left(0.95 * \left(\frac{x}{440}\right)^2 + 0.17 * \frac{x}{440}\right)$$

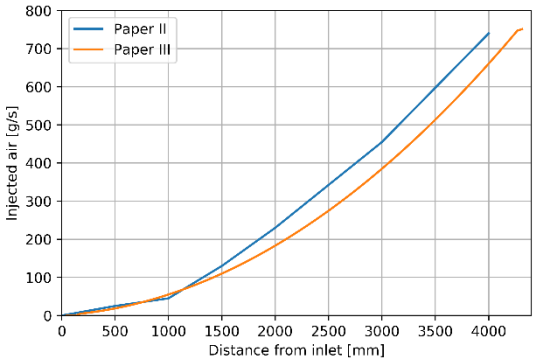

Figure 1. Mixing profiles in Paper II and Paper III

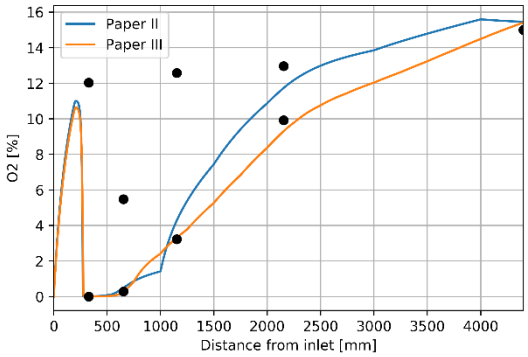

Figure 2. O2 profiles in Paper II and Paper III

APPENDIX C

Temperature measurements of Coal A

The figure below shows the temperature measurement of Coal A in the pilot-scale kiln, as measured by the suction pyrometer and by an IR-camera. Coal A* refers to when Coal A was fired with a low amount of primary air, leading to an attached flame. This is the temperature profile that has been used for most simulations of Coal A in this work. The other case (Coal A) refers to when the amount of primary air was high and resulted in a lifted flame. As can be seen, the temperature is significantly lower when the flame is not attached to the burner.